HHS Public Access

Author manuscript

Biomaterials. Author manuscript; available in PMC 2021 February 01.

Published in final edited form as:

Biomaterials. 2020 February ; 230: 119641. doi:10.1016/j.biomaterials.2019.119641.

Evolution of metallic cardiovascular stent materials: *a comparative study among stainless steel, magnesium and zinc*

Jiayin Fu[1,#], **Yingchao Su**[2,#], **Yi-Xian Qin**[2], **Yufeng Zheng**[3], **Yadong Wang**[1,*], **Donghui Zhu**[2,*]

[1]Nancy E. and Peter C. Meinig School of Biomedical Engineering, Cornell University, Ithaca, NY, USA.

[2]Department of Biomedical Engineering, Stony Brook University, Stony Brook, NY, USA.

[3]Department of Materials Science and Engineering, College of Engineering, Peking University, Beijing, China.

Abstract

A cardiovascular stent is a small mesh tube that expands a narrowed or blocked coronary artery. Unfortunately, current stents, regardless metallic or polymeric, still largely fall short to the ideal clinical needs due to late restenosis, thrombosis and other clinical complications. Nonetheless, metallic stents are preferred clinically thanks to their superior mechanical property and radiopacity to their polymeric counterparts. The emergence of bioresorbable metals opens a window for better stent materials as they may have the potential to reduce or eliminate late restenosis and thrombosis. In fact, some bioresorbable magnesium (Mg)-based stents have obtained regulatory approval or under trials with mixed clinical outcomes. Some major issues with Mg include the too rapid degradation rate and late restenosis. To mitigate these problems, bioresorbable zinc (Zn)-based stent materials are being developed lately with the more suitable degradation rate and better biocompatibility. The past decades have witnessed the unprecedented evolution of metallic stent materials from first generation represented by stainless steel (SS), to second generation represented by Mg, and to third generation represented by Zn. To further elucidate their pros and cons as metallic stent materials, we systematically evaluated their performances *in vitro* and *in vivo* through direct side-by-side comparisons. Our results demonstrated that tailored Zn-based material with proper configurations could be a promising candidate for a better stent material in the future.

[*]Corresponding to: yw839@cornell.edu (Y. Wang), Donghui.Zhu@stonybrook.edu (D. Zhu).
[#]These authors contributed equally to this work.

Declaration of competing interest

The authors declare no competing financial interest.

Data statement

The manuscript includes required protocols in detail and data for reproducibility.

Declaration of interests

The authors declare that they have no known competing financial interests or personal relationships that could have appeared to influence the work reported in this paper.

Graphical Abstract

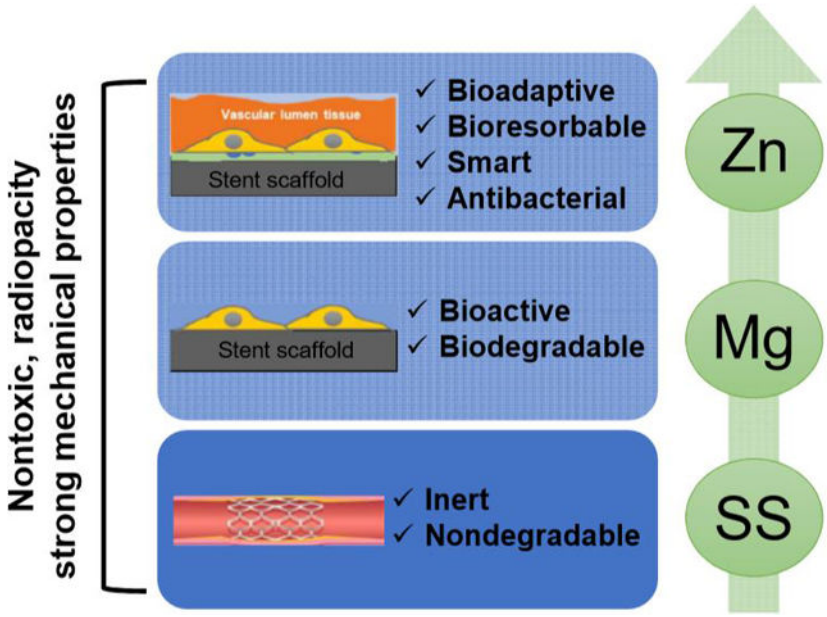

Keywords

Stainless Steel; Magnesium; Zinc; Degradation; Biocompatibility; Antibacterial

INTRODUCTION

Coronary artery disease is the number one cardiovascular disease, which causes around 18 million of death globally [1]. Coronary stent implantation could provide intra-arterial support during the angiographic and other clinical treatments and significantly reduce the post-operative blood vessel restenosis. An ideal coronary stent system requires a combination of several key characteristics for the stent materials [2]. They should have sufficient mechanical strength and ductility to support and conform to an atherosclerotic arterial wall. They should also be biocompatible to avoid the platelet adhesion and plaque formation, which are the main reasons for thrombosis and restenosis. Antibacterial property is another useful characteristic of a stent material, as it can reduce the chance of infection after implantation [3].

Based on these criteria, non-degradable bare metallic stent (BMS) is used as the first-generation stent because of their superior mechanical properties to their polymeric counterparts. 316L stainless steel (SS316L, ASTM F138) is the most common material due to a combination of durability, processability, corrosion resistance and biocompatibility [2, 4]. Cobalt-chromium and nickel-titanium alloys are the other representative materials [2]. Although the BMS can significantly reduce the initial thrombosis, there are long-term complications after stent implantation including chronic inflammation and neointimal hyperplasia leading to thrombosis and restenosis at the late stage of stent placement. To reduce BMS-related restenosis, drug-eluting stents (DES) is developed which can load and

deliver drugs, such as sirolimus and paclitaxel, through polymer coatings on the surfaces of BMS [2, 5–8]. However, as a permanent implant in blood vessels, DES could still result in late thrombosis, restenosis, and chronic inflammation 1 year or 2 after implantation.

Different from BMS and DES, bioresorbable stent is a promising concept that it will degrade spontaneously after implantation and then be completely resorbed with the regeneration of vascular tissues, leading to a fully recovery of blood vessels [9]. This offers an innovative strategy to potentially eliminate the late thrombosis and restenosis caused by non-degradable stent materials. Bioresorbable stents can be made of biodegradable polymers or metals. Poly-L-lactic acid (PLLA) is the most typical polymer used for bioresorbable stents [2, 10]. A critical advantage of the biodegradable polymer stent is that molecular drugs can be released at a slower rate and for a prolonged period [5]. However, thicker stent struts are always the prerequisite for polymer stent in order to retaining sufficient mechanical property during degradation [2]. In addition, biodegradable polymer stents are associated with an increased risk of inflammatory reactions and neointima hyperplasia induced by their degradation products [11, 12].

To mitigate the mechanical and biological problems associated with polymers, biodegradable metallic stents are being developed with alloys based on iron (Fe) and magnesium (Mg) in the past decades [13]. Prior studies have shown that Fe-based stents have good mechanical property and biocompatibility [14, 15], but they degrade too slow and the firm degradation products (largely iron oxide) are retained in the encapsulating neointima and thus deteriorate vascular tissue regeneration [16, 17]. Mg alloys also possess somewhat good mechanical property and good biocompatibility as stent materials [4, 18–21]. Although there are concerns about the rapid degradation of Mg, numerous Mg alloys have been fabricated with improved degradation resistance. WE43 alloy is one of them and used as a commercial product “Lekton Magic Coronary Stent” [22]. However, some major issues still exist with Mg stent materials including the too rapid degradation rate and late restenosis. Compared to Fe and Mg, zinc (Zn) is a new generation of biodegradable stent material with a more suitable degradation rate *in vivo* [16, 23–26]. Similar to Fe and Mg, Zn is also one of the essential trace elements with critical biological roles in human body [23, 27–30]. Although the overdosed release of Zn ions from Zn alloys could potentially result in cytotoxicity to several mammal cell lines [31–33], it usually shows good *in vivo* biocompatibility in several animal models [24, 34].

Although the metallic stent materials evolve rapidly over the past decades, those different generations of metals represented by SS, Mg and Zn respectively are still the main players in the field. They all have their different properties and features, and the purpose of this study is to directly compare their mechanical properties, degradation behaviors, vascular biocompatibility, and antibacterial properties *in vitro* and *in vivo* as metallic cardiovascular stent materials. This side-by-side systematical comparison will elucidate the relationship between their intrinsic properties and extrinsic features, and pinpoint their different benefits and limitations as stent materials.

MATERIALS AND METHODS

Materials

SS316L, Mg-Y-Nd-Zr alloy (WE43 commercial Mg alloy) and 99.99+% pure Zn rod materials (Goodfellow Ltd. Pennsylvania) were cut into discs with diameter of 10 mm and thickness of 5 mm for *in vitro* degradation tests, while the corresponding wire materials (Goodfellow Ltd. Pennsylvania) with a diameter of 0.25 mm were used in the *in vivo* implantation test. All disc samples were polished using #1200 sandpaper and cleaned by sonication in acetone for 5 min before use.

In vitro degradation test

All the degradation tests were carried out in a modified Hanks' solution at 37 ± 0.5 °C [35, 36]. The electrochemical degradation behaviors were measured in a standard three-electrode cell using a Princeton Versa Stat3 electrochemistry workstation [37, 38]. The sample with an exposed surface area of 0.2826 cm^2 was applied as working electrode, and an Ag/AgCl saturated KCl electrode and platinum plate were used as reference electrode and counter electrode, respectively. Briefly, open circuit potential (OCP) was measured during the initial 10 min to achieve a stable potential, and then the electrochemical impedance spectroscopy (EIS) test was performed over a frequency range of 0.01 Hz to 100 kHz with a potential amplitude of 10 mV. The potentiodynamic polarization behaviors were measured at a scan rate of 1 mV/s. The corrosion rate (CR, mm/y) was calculated based on the electrochemical corrosion current density (i_{corr}, μA/cm^2) according to the following equation [37, 39]:

$$CR_i = 3.27 \times 10^{-3} \cdot \frac{i_{corr}}{\rho} EW$$

where ρ is the material density (g/cm^3) and EW is the corresponding equivalent weight (g).

The immersion degradation tests were performed for 1 and 3 months according to a previous study [36]. Briefly, the pH values of the solution with different samples were monitored and were also measured during the immersion tests. The surface morphologies and phase composition of degraded samples after 1 and 3 months of immersion were tested with SEM and XRD. The CR_W (mm/y) was calculated based on weight loss (W_{loss}, mg) according to the following equation [40]:

$$CR_W = 87.06 \times \frac{W_{loss}}{\rho A t}$$

where ρ is the material density (g/cm^3), t is immersion time (h), A is sample surface area (cm^2).

Hemocompatibility

The hemolysis tests and platelet adhesion tests were performed according to the method described previously [41, 42]. In brief, healthy human blood (anticoagulant with 3.8% citric acid sodium, Zen-Bio, US) was diluted by 0.9% sodium chloride solution with a volume

ratio of 4:5. All samples were pre-cultured with 9.8 ml 0.9% sodium chloride solution at 37 °C for 30 min and 0.2 mL diluted blood was then added to each tube and incubated at 37 °C for 60 min. Deionized water and 0.9% sodium chloride solution were incubated with 0.2 mL diluted blood as the positive and negative control, respectively. After centrifuging at 3,000 rpm for 5 min, the supernatants were collected in 96-well plates and the absorbance (A) was measured by a plate reader (Cytation 5, Biotek, US) at 545 nm. The hemolysis rate (HR) was calculated by the following equation: Hemolysis = $(A_{sample} - A_{negative})/(A_{positive} - A_{negative})$.

Platelet rich plasma (PRP) with 10^8/μl platelets (Zen-Bio, US) was used for platelet adhesion test. 50 μl PRP was overlaid on each sample surface and incubated at 37 °C for 1 hour. After gently rinsed by PBS for 3 times to remove the non-adherent platelets, adherent platelets on samples were fixed with 4% paraformaldehyde (PFA, Affymetrix, US) and 2% glutaraldehyde solution (Fisher Chemical, US) at room temperature for 2 h, then dehydrated with gradient alcohol solution (30%, 50%, 70%, 90%, and 100%) and hexamethyldisilazane (HMDS) for 10 min, respectively, and finally dried in desiccator. The samples were coated with gold and observed by SEM. The number of adherent platelets was counted on at least five different SEM images for each sample.

Cytocompatibility

Human endothelial cells (EA.hy926, ATCC CRL-2922, US) and human aortic vascular smooth muscle cells (HA-VSMCs, ATCC CRL-1999, US) were cultured in 75 cm^2 flask (BD Bioscience) with Dulbecco's Modified Eagle Medium (DMEM, ATCC, US) containing 10 % fetal bovine serum (FBS, ScienCell) and 1% penicillin/ streptomycin solution (P/S, ScienCell) [43–45]. For the indirect assays, extract media was prepared by incubating samples in the corresponding cell culture media at a ratio of 1.25 cm^2/mL for 3 days. Afterward, the collected extract solution was diluted with culture media to specific concentrations of 50% and 25%. The cell viability was measured with the MTT assay (Thermo Fisher Scientific, US) after cell culture for 1, 3, and 5 days [46, 47].

Cells with a density of 1×10^5/well were seeded onto different samples with and without being precultured in DMEM for 3 days in a 24 well plate. After 3 days of cell culture, the cell morphology was observed by SEM after being fixed and dehydration in the same method with the platelet adhesion test as described above.

Antibacterial property

Escherichia coli (*E. coli*, ATCC 25922, US) and *Staphylococcus aureus* (*S. aureus*, ATCC 29213, US) were cultured according to the procedures in a previous study [48]. Briefly, the bacteria were cultured in Tryptic Soy Broth (TSB) media at 37 °C and 220 rpm to reach the optical density of 0.5–0.6 at 600 nm. The antibacterial performance was tested with the same procedures in our previous study [49]. 2 ml of the diluted bacterial suspension with a concentration of 5×10^5 /mL in TSB media was incubated with samples for 24 h at 37 °C and 120 rpm. Diluted bacterial suspension without samples was used as negative control. The absorbance of the collected bacteria suspension was read at 600 nm. Antibacterial rates in the TSB media were calculated with the following equation: Antibacterial rates =

($A_{negative} - A_{sample}$) / $A_{negative}$. Before the SEM imaging, samples were fixed and dehydrated with the same procedures with the platelet adhesion test as described above.

In vivo vascular implantation

All procedures were approved by the IACUC at the Cornell University following NIH guidelines for the care and use of laboratory animals. Male young CD IGS rats (strain code: 001, 8–10 weeks, body weight = 300–325 grams, Charles River Laboratories, Boston, MA) were used for metallic wire implantation (n=3 for each different implant at each time point). Rats were anesthetized by isoflurane inhalation (5% for induction, then 1.5% for maintenance). A midline of the abdominal incision was made to expose the abdominal aorta. The aorta was separated from the inferior vena cava. Blood flow of aorta was blocked with a microvascular clamp. SS, Mg alloy or Zn wire were cleaned in ethanol, autoclaved and immersed in heparin solution (1 mg/mL in saline) overnight prior to implantation. Metallic wires were inserted into the distal parts of the aorta with middle parts of the wires (6–8 mm in length) within the lumen and two ends (1–2 mm in length) outside of arterial walls. The microvascular clamp was then removed from the aorta to recover the blood flow. The surgical site was closed with absorbable sutures. No anticoagulation or antiplatelet treatments were administrated pre- and post-operatively. Analgesic (Buprenex, 0.05 mg/kg) was given once before the surgery and every 8 hours for 48 hours.

Patency monitoring with ultrasonography

VisualSonics Vevo-2100 High-Resolution Ultrasound was used to monitor the implanted metallic wires and blood flow in the parts of abdominal aortas that placed with the wires at week 2, 4, 12, and 24 after implantation. Animals were anesthetized with 3% isoflurane in 1L/minute oxygen flow. The hair on the abdomen area was removed with hair removal cream and warm ultrasound gel was then applied to the skin before imaging. Ultrasound detector MS 400 was used for ultrasound imaging at a frequency of 30 MHz. B-mode, color Doppler mode, and PW mode images in cross-section planes were acquired. Aorta patency was determined from color Doppler mode images and flow rate was measured from PW mode images.

X-ray micro-computed tomography (micro-CT)

In vivo degradation of metallic wires was evaluated by high-resolution micro-CT (GE eXplore CT-120) at week 2, 4, 8, 12, and 24 after implantation. Animals were anesthetized with 3% isoflurane in 1L/minute oxygen flow and then CT scanning was performed. For enhanced micro-CT, 1 mL 76% Iopamidol (ISOVUE-370, Bracco Diagnostics, USA) was injected through the rat tail vein prior to scanning. For each metallic wire, 100 scanning planes were obtained and only the middle 50 scanning planes were used to calculate the volume of metallic wire. *In vivo* degradation of metallic wires was defined as a ratio of metallic wire volume at each time point to metallic wire volume before implantation and expressed as a percentage.

Vascular explantation and histological analysis

2, 4 and 24 weeks after metallic wire aortic implantation, rats were anesthetized, and a midline incision of the abdomen was made to expose the abdominal aorta. The aorta including metallic wire was taken out from surrounding tissues for analysis. The explanted wire/aorta was rinsed with sterile PBS, fixed in 4% PFA at 4°C for 1 h, and soaked in 30% sucrose solution at 4°C for 24 h. The whole wire/aorta was embedded vertically into the optimal cutting temperature compound (Sakura Finetek, Torrance, CA), snap-frozen at −80°C, and cryosectioned at 10 μm thickness. Slides were stained with hematoxylin and eosin (H&E) to assess inflammation responses of vascular tissues that surrounded the wires. Picro-sirius red staining was performed to evaluate composition and packing of collagen fibers that encapsulated the metallic wires. All histological images were captured with an inverted microscope (Eclipse Ti2, Nikon, Japan).

Immunofluorescence staining

Tissue sections (10 μm thick) were first blocked with 1% bovine serum albumin (BSA, Sigma-Aldrich) for 30 minutes and then incubated with CD11b primary antibody (mouse monoclonal IgG1, MA1–80560, Thermo Fisher Scientific, USA) in 1% BSA overnight at 4°C. CD11b is a marker for pan-white blood cells. After that, samples were washed twice with PBS and incubated with goat anti-mouse secondary antibody, Alexa Fluor 594 (A-11032, Thermo Fisher Scientific, USA) for 1 hour at room temperature. Nuclei were counterstained with 4', 6-diamidino-2-phenylindole (DAPI, Krackeler Scientific, USA). Tissue sections without primary antibody incubation were used as negative controls. The stained samples were imaged with the inverted microscope.

Statistical analysis

All data were presented as mean ± standard deviation. Each assay had at least three replicates and repeated 3 times independently. One-way or two-way ANOVA followed by Turkey's post-hoc test or two-tailed Student-t test, as appropriate, was used to analyze the statistical significance. $P < 0.05$ was considered as statistically significant.

RESULTS

Mechanical property

Mechanical property is one of the most significant advantages for metallic materials compared to their polymeric counterparts. Fig. 1 summarizes different mechanical properties of SS, Mg, and Zn based materials [19, 33, 50–71]. The SS materials show superior tensile, fatigue and creep strengths to Mg and Zn materials. The Mg and Zn materials have similar tensile and fatigue strengths(Fig. 1 a, b, d), while the Mg materials possess higher creep strengths than Zn materials (Fig. 1 e). The elongation rates of Zn materials showed a discrete distribution with the average value between SS and Mg materials (Fig. 1 c). All three materials can meet the minimal mechanical strength as a stent material even though Mg and Zn may need some proper alloying with some mechanical/thermal treatments. In addition, the mechanical stability is characterized with the percentage of retained strength over the degradation time. The inert SS materials can keep their strength stability during the

implantation. The Zn materials have little decrease on their strength after 2 weeks of degradation and keep around 80% of strength in 8 weeks [33]. The Mg materials loss around 20 % and 35% of their strength in 2 and 8 weeks, respectively [69–71].

In vitro degradation behavior

In order to compare the degradation behaviors of different materials, electrochemical and immersion corrosion tests were applied, and the results are shown in Fig. 2 and 3, respectively. The three metallic materials showed significantly different corrosion behaviors. The OCP and corrosion potential of Zn material were between those of SS and Mg materials (Fig. 2 a–b). The corrosion current density (i_{corr}) and corrosion rate (*CR*) of Mg material were around 20 and 500 times higher than those of Zn and SS material, respectively (Fig. 2 b–c). The different shapes and semicircles diameters of electrochemical impedance spectroscopy (EIS) Nyquist plots in Fig. 2d–f also indicated their different corrosion behaviors. There is only one capacitance loop for SS and Zn materials, indicating their stable surfaces, while the two capacitance loops for Mg material refer to the double layer capacitor of the corrosion product film on the Mg surface. The semicircle diameter for the SS material was much larger than those of Zn and Mg materials, indicating its significantly higher corrosion resistance, consistent with the OCP and polarization results in Fig. 2 a–c.

The surface morphology, composition and pH changes of different materials after 1 and 3 months of immersion in Hanks' solution are shown in Fig. 3. The SS surface showed little change after 1 month of immersion with some corrosion pits appeared on the surface after 3 months of immersion (Fig. 3a). The main composition of the small amount of corrosion product was $Fe(OH)_2$ (Fig. 3b). Mg surface showed a severe but uniform corrosion morphology with the formation of cracks and a mineralization layer in 1 month of immersion. The mineralization layer was mainly micro-sized spherical precipitates and flake clusters with the composition of $Mg_3(PO_4)_2$. After 3 months of degradation, a thicker mineralization layer was formed with more cracks and deep pitting. The main composition changed to $Mg_3(PO_4)_2$, $(Ca, Mg)_3(PO_4)_2$ and $Mg(OH)_2$ (Fig. 3b). Compared to SS and Mg materials, the Zn surface showed a localized corrosion behavior with different corrosion morphology in 1 month. Some white spherical precipitates appeared on the slightly degraded surface in the flat area, with a porous and coarse layer made of micro-sized particles and nanowires on the surface of the pitting area. The main degradation product was $Zn_3(PO_4)_2{\cdot}4H_2O$, $CaZn_2(PO_4)_2{\cdot}2H_2O$, and $Zn(OH)_2$ as indicated by the XRD in Fig. 3b. The localized corrosion continued with deeper corrosion pitting and cracks after 3 months of degradation. There were also more corrosion products formed on the surface, which are mainly composed of $CaZn_2(PO_4)_2{\cdot}2H_2O$ and $Zn(OH)_2$.

The corrosion rates of different materials were calculated on the weight loss, as shown in Fig. 3c. The Mg possessed much more rapid corrosion rate than Zn, while the SS showed little corrosion in 3 months of immersion. The pH of the Hanks solution changed with the immersion time in a different way for these three materials, as shown in Fig. 3d. There was no significant change in the solution pH for SS material. The pH sharply increased to over 9 in the initial two weeks for Mg material and stabilized at around 9.5 in the following 3 months because of the formation of the surface mineralization layer (Fig. 3a). The slow

corrosion of Zn material resulted in a slight pH change in the solution, which reached around 8 after 3 months of immersion.

Hemocompatibility

Platelet adhesion and hemolysis tests were conducted to evaluate the hemocompatibility of materials as shown in Fig. 4. The adhered platelets showed long pseudopodia and aggregation on the SS surface, while those on the Mg and Zn surfaces were dispersedly distributed with little spreading (Fig. 4a). The number of adhered platelets on the Mg and Zn surfaces was similar and significantly less than that on the SS surface (Fig. 4b). Compared to the platelet adhesion, the hemolysis rates of the three materials showed a different trend (Fig. 4c). The hemolysis rates of the SS and Zn materials were lower than the hemolysis limit (5%), which is non-hemolytic according to ASTM F 756–08 [72]. The Mg material induced a significantly higher hemolysis rate of around 40%, indicating the material was hemolytic (Fig. 4c).

In vitro cytocompatibility

Both indirect and direct assays were used to test the *in vitro* cytocompatibility of the three materials. Fig. 5 showed the cell viability of endothelial and smooth muscle cells after cultured with different material extracts for 1, 3 and 5 days in a concentration-dependent manner. Cells had over 80% viability after cultured with different concentrations of SS and Mg material extracts. In contrast, cell viability showed a more concentration and time-dependent pattern for Zn extract: higher concentrations of Zn extract and longer culture time, lower cell viability.

Fig. 6 illustrated the direct cell adhesion and morphology of endothelial and smooth muscle cells on different samples with or without pretreatment in the cell culture media for 3 days. The reason to pretreat materials with cell culture media is to mimic the *in vivo* conditions where stents are subject to blood exposure right after implantation. Cells showed good adhesion and highly-spreading morphology on SS material surface with or without the pretreatment in cell culture media. In contrast, cells on Mg and Zn materials showed different adhesion and morphology with and without the media pretreatment. The cells showed round and poorly spreading morphologies on the Mg and Zn surfaces without pretreatment, while the pretreated Mg and Zn surfaces significantly improved the cell adhesion behavior and the cells showed elongated and spreading morphology despite the cracks on the degraded Mg surface. Compared to the endothelial cells, smooth muscle cells showed similar adhesion and morphology on all samples with or without the pretreatment. Overall, smooth muscle cells grew quite well on SS while their growths on Mg and Zn were stressed with less density and flat morphology.

Antibacterial property

The antibacterial performance of different samples was significantly different for the two bacteria strains *E. coli* and *S. aureus*, as shown in Fig. 7. There were numbers of bacteria aggregation and thick biofilms formation of both bacteria strains on the SS surface (Fig. 7a), and the antibacterial rate in the Tryptic Soy Broth (TSB) media were 2% and 4% for *E. coli* and *S. aureus*, respectively (Fig. 7b), indicating poor antibacterial property for SS. Because

of the severe corrosion, a thick and grass-like film was developed on the Mg surface when cultured with the bacteria. Compared to SS, the number of bacteria decreased significantly on the Mg surface, and the antibacterial rate in the TSB media was increased to more than 45% for *E. coli* and around 99% for *S. aureus*. There was also much less bacterial adhesion on the Zn surface than on SS surface. Antibacterial rates in the solution were around 55% and 98% for *E. coli* and *S. aureus*, respectively. The adhered bacterial morphology and number indicated the Mg and Zn could effectively reduce the bacterial adhesion and growth on the surface as well as the bacterial growth and proliferation in the surrounding environment. Moreover, we assessed their antibacterial properties after culture medium pretreatment as well, similar to the cytocompatibility testing aforementioned (Fig. 7c). Not surprisingly, there was no difference for SS with or without pretreatment. However, the antibacterial rate of Mg after pretreatment dropped significantly to around 15% for both strains, and in contrast, that of Zn only decreased slightly, indicating the different antibacterial mechanisms for these two materials.

Metallic wire abdominal aorta implantation

Next, to evaluate the *in vivo* degradation and biocompatibility of different stent materials in a coronary artery-mimicking environment, a metallic wire abdominal aorta implantation model in rats was used (Fig. 8). The overall survival rate was 100% (9/9) for Mg group, 81.8% (9/11) for Zn group, and 100% (10/10) for SS group. One rat in SS group developed into hindlimb paralysis one day post-operatively and was thus excluded from the SS group. For each group, 70–80% of the metallic wires were inserted into the abdominal aorta with two ends outsides of vascular walls (Fig. 8a). When the samples were collected on week 2 and 4 respectively, metallic wires in each group could be easily identified, which proves the validity of such animal model. The Zn and SS wires still could be observed with fibrotic capsules on the two ends on week 24 (Fig. 8a, arrows), while the Mg wires on week 24 were almost invisible with only residuals after absorption left (Fig. 8a, dash square), suggesting a complete degradation of such materials *in vivo* (Fig. 8a). Ultrasound imaging on week 2 showed the implanted metallic wires all were well fixed into the aortas, as indicated by a white linear shadow left by ultrasound going through metallic wires from top to the bottom (Fig. 8b, arrow heads). Color mode imaging showed red blood flow in aorta while blue blood flow in vena cava (Fig. 8b), suggesting that the aortas were still patent after metallic wire interstation. This result was confirmed by PW mode imaging which showed waves of blood flows (Fig. 8b). The aortas were patent during the whole 24-week experimental period. However, ultrasound shadows caused by metallic wires disappeared on week 24 for Mg group (Fig. 8b), which indicates a complete degradation of the Mg metallic wires. This result was consistent with the macroscopic findings in Fig. 8a. The speed of blood flow in the aortas showed a decreased trend for all the groups (Fig. 8c), which is probably due to metallic wire insertion.

In vivo degradation

To evaluate the *in vivo* degradation of metallic wires in the abdominal aorta, μCT was performed at the designated time pointed. Contrast reagents (red) co-localized the with metallic wires, as shown in enhanced CT in Fig. 9a, which confirms that the metallic wires were in the abdominal aorta. Common CT showed the relative position of metallic wires in

the abdomen of rats (Fig. 9b). Compared with Zn and SS, Mg has a quite close density to surrounding tissues and thus couldn't be clearly revealed in CT. Fig. 9c showed the representative images of metallic wire degradation in the abdominal aorta. From week 2 to week 8, Mg wires quickly lost their mass and showed discontinuous segments (Fig. 9c, arrows). These Mg wires completely lost their structure integrity from week 12 to week 24. Although Zn wires showed discontinuous segments from week 12 to week 24, the structure integrity was still well maintained. While for SS wires, no obvious changes could be observed from the whole experimental period. 50% of the metallic wires from the center (Fig. 9b) were analyzed to quantify metal degradation in the abdominal aorta. As shown in Fig. 9d, Mg wires showed the fastest degradation profile and completely degraded by week 24. Zn wires degraded 40% of their mass after 24-week vascular insertion, while SS wires had the slowest degradation and only degraded 10% of their total mass over the whole experimental period.

Host immune responses

To assess host immune responses to metallic wires in the abdominal aorta, H&E were stained to sections of metallic wires in the vascular walls and lumens, respectively. For vascular walls with metallic wire insertion, all the groups showed fibrotic encapsulation around metallic wires on week 2 and 4 (Fig. 10a). Inflammation responses in Mg group totally resolved with only some fibrotic tissue residues that could be seen on week 24. However, inflammation responses aggravated and caused necrosis of the surrounding tissues in Zn and SS group on week 24. The inflammation responses at the site where metallic wires were in the lumen were much less then vascular walls with metallic wire insertion for all the groups and the fibrotic encapsulation formed on week 2 mostly disappeared on week 4 (Fig. 10b). However, the fibrotic encapsulation and necrosis around metallic wires persisted in Zn and SS group till week 24, while Mg group showed almost normal morphologies of vascular walls.

To characterize the composition and packing of collagen fibers in vascular walls and fibrotic encapsulation surrounding metallic wires, samples were further stained with picro-sirius red. From week 4 to week 24, Mg group showed thicker (red) and densely packed collagen fibers than Zn and SS groups in the vascular walls with metallic wire insertion (Fig. 11a). At the site where metallic wires were in the lumen, Mg group also showed thicker (red) and densely packed collagen fibers in the vascular walls than Zn and SS groups on week 4 (Fig. 11b). On week 24, Zn and SS groups still had thin and loosely packed collagen fibers in both vascular walls and fibrotic encapsulation surrounding metallic wires. However, the metallic wires in the Mg group couldn't be identified any longer. CD11b, a pan-maker for inflammatory cells, was also stained to evaluate inflammation responses around the metallic wires. The Mg group showed a decrease in CD11b staining both in the vascular walls with metallic wire insertion and at the site where metallic wires were in the lumen from week 2 to 24 (Fig. 11 c–d). However, both Zn and SS group showed an increase in the staining in the vascular walls with metallic wire insertion, indicating a stronger inflammation response with time (Fig. 11c). In addition, at the site where metallic wires were in the lumen, Zn and SS group showed a consistently strong CD11b staining, which suggests a long-term inflammation response around these two materials (Fig. 11d).

DISCUSSION

Mechanical properties

The outstanding mechanical properties are one of the significant advantages for metallic stent when compared to the polymeric counterparts. As the respective metallic materials of different generations for cardiovascular stent application, SS, Mg, and Zn were chosen in the present study and their characteristic performances *in vitro* and *in vivo* were summarized in Table 1. SS is the traditional BMS material with high mechanical strength and ductility (Fig. 1). Mg and Zn materials could achieve sufficient strength and elongation after a proper alloying and post treatments. Li, Mg, Ca, Sr, Mn, and Cu could be used as the strengthening alloying elements, while hot rolling and extrusion are the two common post treatments [26, 33, 73, 74]. It was shown (Fig. 8) that the blood flow was decreased in the aortas after implantation for all the wire materials, suggesting that the stent must possess strong enough radial strength to support and conform to the arterial wall to restore blood flow [2]. This indicates that radial mechanical strength and elastic recoil on expansion should be an important parameter for a stent product, though they are closely related to the yield strength and elongation to failure [74, 75]. ASTM B939–15 and ASTM F2079–09 are the corresponding standards to specifically evaluate these two properties.

In addition to the static mechanical strength and durability, cyclic fatigue strength and durability are also critical to the stent's stability in the pulsatile conditions [4]. The weak cyclic fatigue strength and creep strength of Zn and Mg materials are the main concerns for their reliability after the implantation (Fig. 1 d–e). Therefore, it remains as a metallurgical challenge for making mechanically strong enough biodegradable metals. Moreover, the decay of mechanical stability during degradation is more critical for biodegradable stents. The moderate degradation rate of Zn helps maintain its good mechanical stability during the early stage of degradation (Fig. 1 f) [33], while the fast degradation of Mg materials results in unstable mechanical integrity [69–71]. A surface modification may help retard the degradation process and provide sufficient mechanical support to the injured tissue in the early stage [76–78].

Degradation behavior

Higher corrosion resistance has been pursued for a long period for traditional inert metals and thus the titanium alloys, SS, and cobalt-chrome alloys with excellent corrosion resistance have been developed rapidly and commercialized as permanent implant materials in many clinic applications [4, 79, 80]. The traditional SS is well-known for its high corrosion resistance. Different from SS as the permanent stent, Mg and Zn are two promising biodegradable metallic materials for biodegradable stents. A suitable degradation rate of biodegradable stents is beneficial for mechanical support and tissue healing. Therefore, corrosion or degradation behavior is one of the most critical criteria to evaluate metallic materials for clinical applications.

In this study, *in vitro* degradation tests including electrochemical corrosion and immersion corrosion measurements provide a complete degradation profile for these three metallic stent materials. We also used a metallic wire abdominal aorta implantation model in rats to

evaluate their biodegradation *in vivo*. This model is relatively easy to create, and animals have a high survival rate with few surgery-associated complications post-implantation. It was shown that the implanted metallic wires stayed well within aortas for at least 24 weeks. This model also allows for simple monitoring with ultrasound and μCT (Fig. 8 and 9). Compared to larger animals such as dogs and sheep, this model provides a low-cost and valuable platform where we can screen metallic stent materials in the arterial circulation and evaluate vascular responses to metals.

SS is generally considered non-degradable material, however, there were still some corrosion pits (Fig. 3a) and slight weight loss (Fig. 9d) in the *in vitro* and *in vivo* degradation tests, respectively. This is consistent with a prior study that the SS316L showed significant corrosion *in vivo* when compared to commercially pure titanium [81]. Moreover, when applied as stent material, the corrosion rate of SS could be accelerated by some minor constituents in blood, e.g. the sulfur contained in amino acids [82, 83]. In addition, inflammatory reactions could also increase the corrosion rate of 316L stainless steel [84]. Therefore, it is possible that the vascular environment and the chronic inflammation surrounding SS wires accelerates the degradation of 316L stainless steel in this study.

Mg materials are well known for their rapid degradation. The WE43 alloy in the present study showed a degradation rate of around 1 mm/y *in vitro* (Fig. 3c) and lost 90% of its mass after 8 weeks and its structures after 12 weeks *in vivo* (Fig. 9). Therefore, it is probably not a good idea to use bare Mg as stent material and further surface modification should be applied to retard its degradation rate [85–88]. A uniform degradation morphology was found on the Mg surface in the present study (Fig. 3a). This is probably due to the optimized extrusion and heat treatment for WE43 Mg materials and is consistent with the previous studies [89–91]. The uniform degradation behavior is implemental for the mechanical integrity and biocompatibility of the stent implants, especially after the coating eroded during the degradation of the Mg stents.

Compared to Mg, Zn has been regarded as a new generation of biodegradable stent materials with a more suitable degradation rate *in vivo* [16, 23–26]. Zn showed a degradation rate of around 0.05 mm/y *in vitro* and lost about 40% of its mass (Fig. 3c) and still kept its intact structures after 24 weeks *in vivo* (Fig. 9), which is a desired degradation rate for clinical stent application. It has been reported that Zn could degrade uniformly in the initial stage of implantation and then evolved to localized degradation [16, 24]. In this study, typically localized degradation morphologies were characterized in the Hanks' solution *in vitro* (Fig. 3a) and in rat abdominal aortas *in vivo* (Fig. 9c). When compared to uniform degradation, localized degradation could result in higher risks on the mechanical failure of the implanted stents. In addition, the blood flow in the aortas showed a decreased trend (Fig. 8), which is probably because the metallic wire insertion and inflammation responses around metallic wires (Fig. 10–11) caused a narrowing of the effective lumen for blood flow in the aortas.

Biocompatibility

For the *in vitro* biocompatibility, the SS material showed excellent cytocompatibility for the viability, adhesion and proliferation of endothelial cells (Fig. 6). However, it activated the platelet adhesion and smooth muscle adhesion (Fig. 4 and 7), which could possibly lead to

the in-stent restenosis after percutaneous intervention [92]. Different from SS, the Mg surface limited the platelet activation and smooth muscle cell proliferation. The Mg material also produced harmless degradation products, which could be confirmed by the improved endothelial cell viability in the extract media (Fig. 5) and cell adhesion and spreading on the degraded surface (Fig. 6). One concern is its high hemolysis rate, which is related to the high pH value and releasing of rare earth elements [93, 94]. Compared to the other two materials, Zn showed an overall better biocompatibility, including less platelet activation and lower hemolysis rate (Fig. 4), acceptable cell viability with the diluted extracts (Fig. 5), good cell adhesion after pretreatment with culture media (Fig. 6), and restrained smooth muscle cell proliferation (Fig. 6). It is noteworthy that the pretreatment with the cell culture media could enhance the cytocompatibility of endothelial cells on biodegradable Mg and Zn materials, which is in agreement with previous studies [95–97]. The pretreatment can help the biodegradable metals to produce a thin layer of degradation products and protein on the surface, which will reduce the degradation rate and subsequent pH change for Mg materials as well as burst metallic ions release for both Zn and Mg materials [23, 49, 98]. Opposite to the endothelial cells, the smooth muscle cell proliferation was still largely restrained on both materials. The endothelial cells selectivity over smooth muscle cells were also observed on Zn-Mg, Ca, Sr alloys and other materials in many previous studies [33, 99–103]. One possible reason could be the different preferences of these two cell types on different surface topography [99, 100] and chemistry [102, 103]. In fact, the bioinspired surface modification with different structures and coatings is a good strategy to induce the selective cell adhesion [99, 103]. Another reason could be that endothelial cells have a high tolerance toward metallic ion than smooth muscle cells. It has been reported that smooth muscle cells have tolerances upper limit of around 20 mM and 40 M to Mg and Zn ion, respectively, much lower than that of endothelial cells, about 40 mM and 60 M, respectively [46, 104–106].

To date, most studies that focus on the behavior of stent material degradation are conducted *in vitro* [104, 107], while most *in vivo* studies that investigate degradation of materials use a subcutaneous model [108, 109]. However, this animal model is not appropriate for evaluating the degradation of stent materials due to a huge difference in biological milieu between the arterial and subcutaneous environment. Compared with *in vitro* studies or *in vivo* subcutaneous models, the value of rat aortic implantation model is that it allows reliable investigation of biodegradation and biocompatibility of novel stent materials, since real metal-blood and metal-vascular matrix interfaces can be created. Many studies have used this animal model as a validation platform to identify promising stent materials or study biocompatibility of new stent materials [110–114], it indeed facilitates the discovery of better candidate stent materials. The study that reports for the first time the possibility of Zn as a bioabsorbable cardiac stent material was using the rat aortic implantation model [114]. We also showed in this study a quite similar result that Zn wires degraded 40% of their mass after 24-week vascular insertion with micro-CT scanning. All these reports highlight the validity of rat aortic implantation model in predicting stent material degradation behavior *in vivo*.

However, a metallic wire just represents a small segment of a stent and cannot simulate all aspects of a stent [112]. For example, one limitation of this model is that it cannot replicate mechanical conditions that a stent is subjected to when deployed in arteries [115]. Thus,

following a quick evaluation of degradation behavior and biocompatibility of candidate stent materials in small animals, stent manufacturing and large animal implantation studies are still required to investigate the degradation behavior of a real stent.

For the *in vivo* inflammation responses in the abdominal aorta, as metallic wires slide when samples (aortas/metallic wires) were cryosectioned prior to staining, so some samples were not intact in structures (Fig. 10–11). The Mg group showed a minimal inflammation response, which was resolved after its complete degradation *in vivo*, while both Zn and SS group demonstrated similar and persistent inflammation responses. In-stent restenosis due to plaque redistribution, thrombosis, and neointimal hyperplasia is the major long-term complications for intracoronary stent placement [2, 116]. Restenosis usually occurs within 6 months after a successful intervention [117, 118]. From H&E results in Fig. 10, due to inflammation responses, we could see fibrotic capsules and necrosis surrounding both Zn and SS wires on week 24. These interesting results indicate that degradability of metal materials for stents is highly desired, as foreign body reaction can continue until the metals completely degrade *in vivo*. As Zn can also degrade *in vivo* with a slower rate than Mg, it is reasonable to speculate that inflammation responses caused by Zn could be resolved eventually after its complete degradation *in vivo*. In addition, the inflammation responses could be reduced by alloying Zn with other elements, which could greatly minimize the occurrence of restenosis. It has been found previously that Zn-Li and Zn-Al alloys caused only moderate inflammation responses in rat abdominal aortas [110, 113]. Therefore, it is possible to improve the biocompatibility of Zn material by alloying with other elements. This study is also the first that compares inflammation responses caused by three different metal materials for stents in a coronary artery-mimicking environment for 6 months. Certainly, these results only revealed what happened when they were implanted in rats, and it could be a completely different story when implanted in other animal models and humans as species do matter.

Antibacterial property

In addition to the degradation and biocompatibility, antibacterial property is another critical criterion for stents, which could help prevent the biofilm formation and infection. As a traditional stent material, SS surface could potentially induce the biofilm formation (Fig. 7a) and require prophylaxis and treatment with antibiotics in the surgery [119]. Mg and Zn materials showed mixed antibacterial performances against the two most common bacterial strains used in this study (Fig. 7), but their antibacterial mechanisms are different. The quick degradation of Mg resulted in dramatic increase of the pH in the media, which induced its high antibacterial rate in Fig. 7b. When the degradation of Mg was slowed by surface pretreatment with culture medium, the antibacterial rate of Mg dropped significantly to only about 15% (Fig. 7c). Thus, the antibacterial mechanism for Mg materials is largely originated from the dramatic pH increase in the surrounding environment due to this fast degradation. The released hydrogen gas could also be useful to reduce the bacterial adhesion on the surface. However, because of its grass-like porous surface after degradation, there was more surface bacterial adhesion than that of Zn (Fig. 7a). Different from Mg, evidence showed that Zn is a potential antibacterial agent in biomaterials as the main component or doping agent [23]. Through the interaction with bacterial surfaces, the released Zn ion could

alter the bacterial cell surface charge balance and induce the bacteriolysis during the degradation of Zn materials [49, 120]. Because of the photocatalytic property of Zn based materials, reactive oxygen species (ROS) generation is another possible antibacterial mechanism [121]. Therefore, a controlled Zn ion release profile is critical to achieving the balance of biocompatibility and antibacterial performances. In addition to Zn ion, the degradation products including ZnO, $Zn(OH)_2$, and zinc-based phosphates (Fig. 3b) could also induce the antibacterial reaction and decrease the bacterial adhesion on the degraded surface [49, 122–124].

CONCLUSIONS

Through the comprehensive study on the past, current and future generation metallic cardiovascular stent materials, *i.e.* SS, Mg, and Zn materials, an *in vitro* and *in vivo* degradation and biocompatibility profile together with the antibacterial performance was provided. The traditional SS materials showed little degradation and excellent endothelial cell compatibility, but the activated platelet and smooth muscle adhesion *in vitro* with persistent inflammation response *in vivo* were potential clinic problems as a permanent stent material. As a biodegradable metallic material, Mg limited the platelet activation and smooth muscle cell proliferation while retaining the cytocompatibility to endothelial cells. Its fast degradation rate was the main concern to bring a high pH change and hemolysis rate. However, through an optimized extrusion and heat treatment, Mg could achieve a uniform degradation and a minimum *in vivo* inflammation. Zn is a new generation of biodegradable stent materials with many benefits for clinical application: ideal degradation rate *in vivo*, comprehensive hemocompatibility and cytocompatibility, and restrained smooth muscle cell proliferation, together with good antibacterial performance. Although Zn showed a similar *in vivo* inflammation response as SS, it is expected to be resolved with the degradation process.

Acknowledgments

This work was supported by National Institutes of Health [Grant number R01HL140562]. The content is solely the responsibility of the authors and does not necessarily represent the official views of the National Institutes of Health. We also thank Yu Wang and Felix Law for their generous help on material preparation and characterization.

REFERENCES

[1]. Roth GA, Johnson C, Abajobir A, Abd-Allah F, Abera SF, Abyu G, Ahmed M, Aksut B, Alam T, Alam K, Alla F, Alvis-Guzman N, Amrock S, Ansari H, Arnlov J, Asayesh H, Atey TM, Avila-Burgos L, Awasthi A, Banerjee A, Barac A, Barnighausen T, Barregard L, Bedi N, Ketema E. Belay, Bennett D, Berhe G, Bhutta Z, Bitew S, Carapetis J, Carrero JJ, Malta DC, Castaneda-Orjuela CA, Castillo-Rivas J, Catala-Lopez F, Choi JY, Christensen H, Cirillo M, Cooper L Jr., Criqui M, Cundiff D, Damasceno A, Dandona L, Dandona R, Davletov K, Dharmaratne S, Dorairaj P, Dubey M, Ehrenkranz R, El Sayed Zaki M, Faraon EJA, Esteghamati A, Farid T, Farvid M, Feigin V, Ding EL, Fowkes G, Gebrehiwot T, Gillum R, Gold A, Gona P, Gupta R, Habtewold TD, Hafezi-Nejad N, Hailu T, Hailu GB, Hankey G, Hassen HY, Abate KH, Havmoeller R, Hay SI, Horino M, Hotez PJ, Jacobsen K, James S, Javanbakht M, Jeemon P, John D, Jonas J, Kalkonde Y, Karimkhani C, Kasaeian A, Khader Y, Khan A, Khang YH, Khera S, Khoja AT, Khubchandani J, Kim D, Kolte D, Kosen S, Krohn KJ, Kumar GA, Kwan GF, Lal DK, Larsson A, Linn S, Lopez A, Lotufo PA, El Razek HMA, Malekzadeh R, Mazidi M, Meier T, Meles KG, Mensah G, Meretoja A, Mezgebe H, Miller T, Mirrakhimov E, Mohammed S, Moran

AE, Musa KI, Narula J, Neal B, Ngalesoni F, Nguyen G, Obermeyer CM, Owolabi M, Patton G, Pedro J, Qato D, Qorbani M, Rahimi K, Rai RK, Rawaf S, Ribeiro A, Safiri S, Salomon JA, Santos I, Milicevic M. Santric, Sartorius B, Schutte A, Sepanlou S, Shaikh MA, Shin MJ, Shishehbor M, Shore H, Silva DAS, Sobngwi E, Stranges S, Swaminathan S, Tabares-Seisdedos R, Atnafu N. Tadele, Tesfay F, Thakur JS, Thrift A, Topor-Madry R, Truelsen T, Tyrovolas S, Ukwaja KN, Uthman O, Vasankari T, Vlassov V, Vollset SE, Wakayo T, Watkins D, Weintraub R, Werdecker A, Westerman R, Wiysonge CS, Wolfe C, Workicho A, Xu G, Yano Y, Yip P, Yonemoto N, Younis M, Yu C, Vos T, Naghavi M, Murray C, Global, Regional, and National Burden of Cardiovascular Diseases for 10 Causes, 1990 to 2015, J Am Coll Cardiol 70(1) (2017) 1–25. [PubMed: 28527533]

[2]. Mani G, Feldman MD, Patel D, Agrawal CM, Coronary stents: a materials perspective, Biomaterials 28(9) (2007) 1689–710. [PubMed: 17188349]

[3]. Zheng YF, Zhang BB, Wang BL, Wang YB, Li L, Yang QB, Cui LS, Introduction of antibacterial function into biomedical TiNi shape memory alloy by the addition of element Ag, Acta Biomater. 7(6) (2011) 2758–2767. [PubMed: 21316493]

[4]. Chen QZ, Thouas GA, Metallic implant biomaterials, Materials Science & Engineering R-Reports 87 (2015) 1–57.

[5]. Peng T, Gibula P, Yao KD, Goosen MF, Role of polymers in improving the results of stenting in coronary arteries, Biomaterials 17(7) (1996) 685–94. [PubMed: 8672630]

[6]. Ma J, Thompson M, Zhao N, Zhu D, Similarities and differences in coatings for magnesium-based stents and orthopaedic implants, Journal of orthopaedic translation 2(3) (2014) 118–130. [PubMed: 27695671]

[7]. Su Y, Luo C, Zhang Z, Hermawan H, Zhu D, Huang J, Liang Y, Li G, Ren L, Bioinspired surface functionalization of metallic biomaterials, J. Mech. Behav. Biomed. Mater 77 (2018) 90–105. [PubMed: 28898726]

[8]. Ma J, Zhao N, Zhu D, Sirolimus-eluting dextran and polyglutamic acid hybrid coatings on AZ31 for stent applications, J. Biomater. Appl 30(5) (2015) 579–88. [PubMed: 26202889]

[9]. Ormiston JA, Serruys PW, Bioabsorbable coronary stents, Circ Cardiovasc Interv 2(3) (2009) 255–60. [PubMed: 20031723]

[10]. Stack R, Califf R, Phillips H, Pryor D, Quigley P, Bauman R, Tcheng J, Greenfield J, Interventional cardiac catheterization at duke medical center-the duke interventional cardiac catheterization program, American Journal of Cardiology 62(10 PART II) (1988).

[11]. Su SH, Nguyen KT, Satasiya P, Greilich PE, Tang L, Eberhart RC, Curcumin impregnation improves the mechanical properties and reduces the inflammatory response associated with poly(L-lactic acid) fiber, J Biomater Sci Polym Ed 16(3) (2005) 353–70. [PubMed: 15850289]

[12]. van der Giessen WJ, Lincoff AM, Schwartz RS, van Beusekom HM, Serruys PW, Holmes DR Jr., Ellis SG, Topol EJ, Marked inflammatory sequelae to implantation of biodegradable and nonbiodegradable polymers in porcine coronary arteries, Circulation 94(7) (1996) 1690–7. [PubMed: 8840862]

[13]. Moravej M, Mantovani D, Biodegradable metals for cardiovascular stent application: interests and new opportunities, Int. J. Mol. Sci 12(7) (2011) 4250–70. [PubMed: 21845076]

[14]. Peuster M, Wohlsein P, Brugmann M, Ehlerding M, Seidler K, Fink C, Brauer H, Fischer A, Hausdorf G, A novel approach to temporary stenting: degradable cardiovascular stents produced from corrodible metal - results 6–18 months after implantation into New Zealand white rabbits, Heart 86(5) (2001) 563–569. [PubMed: 11602554]

[15]. Huang T, Cheng J, Zheng YF, In vitro degradation and biocompatibility of Fe-Pd and Fe-Pt composites fabricated by spark plasma sintering, Mater Sci Eng C Mater Biol Appl 35 (2014) 43–53. [PubMed: 24411350]

[16]. Bowen PK, Drelich J, Goldman J, Zinc exhibits ideal physiological corrosion behavior for bioabsorbable stents, Adv. Mater 25(18) (2013) 2577–82. [PubMed: 23495090]

[17]. Pierson D, Edick J, Tauscher A, Pokorney E, Bowen P, Gelbaugh J, Stinson J, Getty H, Lee CH, Drelich J, Goldman J, A simplified in vivo approach for evaluating the bioabsorbable behavior of candidate stent materials, J Biomed Mater Res B Appl Biomater 100(1) (2012) 58–67. [PubMed: 21905215]

[18]. Erbel R, Di Mario C, Bartunek J, Bonnier J, de Bruyne B, Eberli FR, Erne P, Haude M, Heublein B, Horrigan M, Ilsley C, Bose D, Koolen J, Luscher TF, Weissman N, Waksman R, Investigators P-A, Temporary scaffolding of coronary arteries with bioabsorbable magnesium stents: a prospective, non-randomised multicentre trial, Lancet 369(9576) (2007) 1869–1875. [PubMed: 17544767]

[19]. Zheng YF, Gu XN, Witte F, Biodegradable metals, Materials Science and Engineering: R: Reports 77(0) (2014) 1–34.

[20]. Zhao N, Zhu D, Bioscaffolds development for small-diameter vascular grafts, Int. J. Biomed. Eng. Technol 12(2) (2013) 113–129.

[21]. Zhao N, Zhu D, Application of Mg-based alloys for cardiovascular stents, Int. J. Biomed. Eng. Technol 12(4) (2013) 382–398.

[22]. Di Mario C, Griffiths H, Goktekin O, Peeters N, Verbist J, Bosiers M, Deloose K, Heublein B, Rohde R, Kasese V, Ilsley C, Erbel R, Drug-eluting bioabsorbable magnesium stent, J Interv Cardiol 17(6) (2004) 391–5. [PubMed: 15546291]

[23]. Su Y, Cockerill I, Wang Y, Qin YX, Chang L, Zheng Y, Zhu D, Zinc-Based Biomaterials for Regeneration and Therapy, Trends Biotechnol. 37(4) (2019) 428–441. [PubMed: 30470548]

[24]. Yang H, Wang C, Liu C, Chen H, Wu Y, Han J, Jia Z, Lin W, Zhang D, Li W, Yuan W, Guo H, Li H, Yang G, Kong D, Zhu D, Takashima K, Ruan L, Nie J, Li X, Zheng Y, Evolution of the degradation mechanism of pure zinc stent in the one-year study of rabbit abdominal aorta model, Biomaterials 145 (2017) 92–105. [PubMed: 28858721]

[25]. Zhu D, Su Y, Young ML, Ma J, Zheng Y, Tang L, Biological Responses and Mechanisms of Human Bone Marrow Mesenchymal Stem Cells to Zn and Mg Biomaterials, ACS Appl Mater Interfaces 9(33) (2017) 27453–27461. [PubMed: 28787130]

[26]. Bowen PK, Shearier ER, Zhao S, Guillory RJ 2nd, Zhao F, Goldman J, Drelich JW, Biodegradable Metals for Cardiovascular Stents: from Clinical Concerns to Recent Zn-Alloys, Adv Healthc Mater 5(10) (2016) 1121–40. [PubMed: 27094868]

[27]. Zhu D, Su Y, Zheng Y, Fu B, Tang L, Qin YX, Zinc regulates vascular endothelial cell activity through zinc-sensing receptor ZnR/GPR39, Am J Physiol-Cell Ph 314(4) (2018) C404–C414.

[28]. McCall KA, Huang CC, Fierke CA, Function and mechanism of zinc metalloenzymes, J Nutr 130(5) (2000) 1437s–1446s. [PubMed: 10801957]

[29]. Qiao Y, Zhang W, Tian P, Meng F, Zhu H, Jiang X, Liu X, Chu PK, Stimulation of bone growth following zinc incorporation into biomaterials, Biomaterials 35(25) (2014) 6882–97. [PubMed: 24862443]

[30]. Little PJ, Bhattacharya R, Moreyra AE, Korichneva IL, Zinc and cardiovascular disease, Nutrition 26(11–12) (2010) 1050–7. [PubMed: 20950764]

[31]. Zhang D, Wong CS, Wen C, Li Y, Cellular responses of osteoblast-like cells to 17 elemental metals, Journal of biomedical materials research. Part A 105(1) (2017) 148–158. [PubMed: 27601355]

[32]. Shearier ER, Bowen PK, He W, Drelich A, Drelich J, Goldman J, Zhao F, In Vitro Cytotoxicity, Adhesion, and Proliferation of Human Vascular Cells Exposed to Zinc, Acs Biomater Sci Eng 2(4) (2016) 634–642. [PubMed: 27840847]

[33]. Li HF, Xie XH, Zheng YF, Cong Y, Zhou FY, Qiu KJ, Wang X, Chen SH, Huang L, Tian L, Qin L, Development of biodegradable Zn-1X binary alloys with nutrient alloying elements Mg, Ca and Sr, Scientific reports 5 (2015) 10719. [PubMed: 26023878]

[34]. Bowen PK, Guillory RJ 2nd, Shearier ER, Seitz JM, Drelich J, Bocks M, Zhao F, Goldman J, Metallic zinc exhibits optimal biocompatibility for bioabsorbable endovascular stents, Mater Sci Eng C Mater Biol Appl 56 (2015) 467–72. [PubMed: 26249616]

[35]. Levesque J, Hermawan H, Dube D, Mantovani D, Design of a pseudo-physiological test bench specific to the development of biodegradable metallic biomaterials, Acta Biomater. 4(2) (2008) 284–95. [PubMed: 18033745]

[36]. Su YC, Champagne S, Trenggono A, Tolouei R, Mantovani D, Hermawan H, Development and characterization of silver containing calcium phosphate coatings on pure iron foam intended for bone scaffold applications, Mater Design 148 (2018) 124–134.

[37]. Shi ZM, Atrens A, An innovative specimen configuration for the study of Mg corrosion, Corros. Sci 53(1) (2011) 226–246.

[38]. Su YC, Li GY, Lian JS, A Chemical Conversion Hydroxyapatite Coating on AZ60 Magnesium Alloy and Its Electrochemical Corrosion Behaviour, Int. J. Electrochem. Sci 7(11) (2012) 11497–11511.

[39]. Su YC, Guo YT, Huang ZL, Zhang ZH, Li GY, Lian JS, Ren LQ, Preparation and corrosion behaviors of calcium phosphate conversion coating on magnesium alloy, Surf Coat Tech 307 (2016) 99–108.

[40]. A. G31–12a, Standard Guide for Laboratory Immersion Corrosion Testing of Metals, ASTM West Conshohocken, PA, 2012.

[41]. Yang H, Qu X, Lin W, Wang C, Zhu D, Dai K, Zheng Y, In vitro and in vivo studies on zinc-hydroxyapatite composites as novel biodegradable metal matrix composite for orthopedic applications, Acta Biomater. 71 (2018) 200–214. [PubMed: 29530820]

[42]. Gu X, Zheng Y, Cheng Y, Zhong S, Xi T, In vitro corrosion and biocompatibility of binary magnesium alloys, Biomaterials 30(4) (2009) 484–98. [PubMed: 19000636]

[43]. Hauser S, Jung F, Pietzsch J, Human Endothelial Cell Models in Biomaterial Research, Trends Biotechnol. 35(3) (2017) 265–277. [PubMed: 27789063]

[44]. Wei Y, Chen F, Zhang T, Chen D, Jia X, Wang J, Guo W, Chen J, A Tubing-Free Microfluidic Wound Healing Assay Enabling the Quantification of Vascular Smooth Muscle Cell Migration, Scientific reports 5 (2015) 14049. [PubMed: 26365412]

[45]. Lv J, Wang L, Zhang J, Lin R, Wang L, Sun W, Wu H, Xin S, Long noncoding RNA H19-derived miR-675 aggravates restenosis by targeting PTEN, Biochem. Biophys. Res. Commun 497(4) (2018) 1154–1161. [PubMed: 28063931]

[46]. Ma J, Zhao N, Zhu D, Endothelial Cellular Responses to Biodegradable Metal Zinc, Acs Biomater Sci Eng 1(11) (2015) 1174–1182. [PubMed: 27689136]

[47]. Ma J, Zhao N, Zhu D, Biphasic responses of human vascular smooth muscle cells to magnesium ion, Journal of biomedical materials research. Part A 104(2) (2016) 347–56. [PubMed: 26402437]

[48]. Robinson DA, Griffith RW, Shechtman D, Evans RB, Conzemius MG, In vitro antibacterial properties of magnesium metal against Escherichia coli, Pseudomonas aeruginosa and Staphylococcus aureus, Acta Biomater. 6(5) (2010) 1869–77. [PubMed: 19818422]

[49]. Su Y, Wang K, Gao J, Yang Y, Qin YX, Zheng Y, Zhu D, Enhanced cytocompatibility and antibacterial property of zinc phosphate coating on biodegradable zinc materials, Acta Biomater. (2019).

[50]. Baddoo NR, Stainless steel in construction: A review of research, applications, challenges and opportunities, J. Constr. Steel Res. 64(11) (2008) 1199–1206.

[51]. Levy G. Katarivas, Goldman J, Aghion E, The Prospects of Zinc as a Structural Material for Biodegradable Implants—A Review Paper, Metals 7(10) (2017) 402.

[52]. Zhou WR, Zheng YF, Leeflang MA, Zhou J, Mechanical property, biocorrosion and in vitro biocompatibility evaluations of Mg-Li-(Al)-(RE) alloys for future cardiovascular stent application, Acta Biomater. 9(10) (2013) 8488–98. [PubMed: 23385218]

[53]. Zhang X, Yuan G, Niu J, Fu P, Ding W, Microstructure, mechanical properties, biocorrosion behavior, and cytotoxicity of as-extruded Mg-Nd-Zn-Zr alloy with different extrusion ratios, J. Mech. Behav. Biomed. Mater 9 (2012) 153–62. [PubMed: 22498293]

[54]. Witte F, Hort N, Vogt C, Cohen S, Kainer KU, Willumeit R, Feyerabend F, Degradable biomaterials based on magnesium corrosion, Current Opinion in Solid State & Materials Science 12(5–6) (2008) 63–72.

[55]. Shi L, Northwood DO, Strain-Hardening and Recovery during the Creep of Pure Polycrystalline Magnesium, Acta Metall. Mater 42(3) (1994) 871–877.

[56]. Somekawa H, Hirai K, Watanabe H, Takigawa Y, Higashi K, Dislocation creep behavior in Mg-Al-Zn alloys, Mat Sci Eng a-Struct 407(1–2) (2005) 53–61.

[57]. Kang DH, Park SS, Kim NJ, Development of creep resistant die cast Mg-Sn-Al-Si alloy, Mat Sci Eng a-Struct 413 (2005) 555–560.

[58]. Zhu SM, Wu CC, Li GN, Zheng YF, Nie JF, Creep properties of biodegradable Zn-0.1Li alloy at human body temperature: implications for its durability as stents, Materials Research Letters 7(9) (2019) 347–353.

[59]. Wang YB, Zeng JM, Effects of Mn addition on the microstructure and indentation creep behavior of the hot dip Zn coating, Mater Design 69 (2015) 64–69.

[60]. Feaugas X, Gaudin C, Ratchetting process in the stainless steel AISI 316L at 300 K: an experimental investigation, Int. J. Plast 20(4–5) (2004) 643–662.

[61]. Wilshire B, Willis M, Mechanisms of strain accumulation and damage development during creep of prestrained 316 stainless steels, Metallurgical and Materials Transactions a-Physical Metallurgy and Materials Science 35a(2) (2004) 563–571.

[62]. Jafari S, Raman RKS, Davies CHJ, Corrosion fatigue of a magnesium alloy in modified simulated body fluid, Eng. Fract. Mech 137 (2015) 2–11.

[63]. Shih TS, Liu WS, Chen YJ, Fatigue of as-extruded AZ61A magnesium alloy, Mat Sci Eng a-Struct 325(1–2) (2002) 152–162.

[64]. Tokaji K, Kamakura M, Ishiizumi Y, Hasegawa N, Fatigue behaviour and fracture mechanism of a rolled AZ31 magnesium alloy, Int. J. Fatigue 26(11) (2004) 1217–1224.

[65]. Zhang P, Lindemann J, Influence of shot peening on high cycle fatigue properties of the high-strength wrought magnesium alloy AZ80, Scr. Mater 52(6) (2005) 485–490.

[66]. Tokaji K, Kohyama K, Akita M, Fatigue behaviour and fracture mechanism of a 316 stainless steel hardened by carburizing, Int. J. Fatigue 26(5) (2004) 543–551.

[67]. Akita M, Tokaji K, Effect of carburizing on notch fatigue behaviour in AISI 316 austenitic stainless steel, Surf Coat Tech 200(20–21) (2006) 6073–6078.

[68]. Agarwal N, Kahn H, Avishai A, Michal G, Ernst F, Heuer AH, Enhanced fatigue resistance in 316L austenitic stainless steel due to low-temperature paraequilibrium carburization, Acta Mater. 55(16) (2007) 5572–5580.

[69]. Bakhsheshi-Rad HR, Idris MH, Abdul-Kadir MR, Ourdjini A, Medraj M, Daroonparvar M, Hamzah E, Mechanical and bio-corrosion properties of quaternary Mg-Ca-Mn-Zn alloys compared with binary Mg-Ca alloys, Mater Design 53 (2014) 283–292.

[70]. Imwinkelried T, Beck S, Iizuka T, Schaller B, Effect of a plasmaelectrolytic coating on the strength retention of in vivo and in vitro degraded magnesium implants, Acta Biomater. 9(10) (2013) 8643–9. [PubMed: 22963846]

[71]. Tan L, Wang Q, Lin X, Wan P, Zhang G, Zhang Q, Yang K, Loss of mechanical properties in vivo and bone-implant interface strength of AZ31B magnesium alloy screws with Si-containing coating, Acta Biomater. 10(5) (2014) 2333–40. [PubMed: 24361529]

[72]. Standard A, Standard practice for assessment of hemolytic properties of materials, F756–08 (2008).

[73]. Venezuela J, Dargusch MS, The influence of alloying and fabrication techniques on the mechanical properties, biodegradability and biocompatibility of zinc: A comprehensive review, Acta Biomater. 87 (2019) 1–40. [PubMed: 30660777]

[74]. Li G, Yang H, Zheng Y, Chen XH, Yang JA, Zhu D, Ruan L, Takashima K, Challenges in the use of zinc and its alloys as biodegradable metals: Perspective from biomechanical compatibility, Acta Biomater. 97 (2019) 23–45. [PubMed: 31349057]

[75]. Pang JC, Li SX, Wang ZG, Zhang ZF, General relation between tensile strength and fatigue strength of metallic materials, Mat Sci Eng a-Struct 564 (2013) 331–341.

[76]. Zhao D, Witte F, Lu F, Wang J, Li J, Qin L, Current status on clinical applications of magnesium-based orthopaedic implants: A review from clinical translational perspective, Biomaterials 112 (2017) 287–302. [PubMed: 27770632]

[77]. Agarwal S, Curtin J, Duffy B, Jaiswal S, Biodegradable magnesium alloys for orthopaedic applications: A review on corrosion, biocompatibility and surface modifications, Mater Sci Eng C Mater Biol Appl 68 (2016) 948–963. [PubMed: 27524097]

[78]. Oliver J.-a.N., Su Y, Lu X, Kuo P-H, Du J, Zhu D, Bioactive glass coatings on metallic implants for biomedical applications, Bioactive Materials 4 (2019) 261–270. [PubMed: 31667443]

[79]. Wang X, Xu S, Zhou S, Xu W, Leary M, Choong P, Qian M, Brandt M, Xie YM, Topological design and additive manufacturing of porous metals for bone scaffolds and orthopaedic implants: A review, Biomaterials 83 (2016) 127–41. [PubMed: 26773669]

[80]. Bonaa KH, Mannsverk J, Wiseth R, Aaberge L, Myreng Y, Nygard O, Nilsen DW, Klow NE, Uchto M, Trovik T, Bendz B, Stavnes S, Bjornerheim R, Larsen AI, Slette M, Steigen T, Jakobsen OJ, Bleie O, Fossum E, Hanssen TA, Dahl-Eriksen O, Njolstad I, Rasmussen K, Wilsgaard T, Nordrehaug JE, Investigators N, Drug-Eluting or Bare-Metal Stents for Coronary Artery Disease, N Engl J Med 375(13) (2016) 1242–52. [PubMed: 27572953]

[81]. Krischak GD, Gebhard F, Mohr W, Krivan V, Ignatius A, Beck A, Wachter NJ, Reuter P, Arand M, Kinzl L, Claes LE, Difference in metallic wear distribution released from commercially pure titanium compared with stainless steel plates, Arch Orthop Trauma Surg 124(2) (2004) 104–13. [PubMed: 14727127]

[82]. Greene ND, Jones DA, Corrosion of Surgical Implants, J Mater 1(2) (1966) 345–&.

[83]. Eliaz N, Corrosion of Metallic Biomaterials: A Review, Materials (Basel) 12(3) (2019).

[84]. Brooks EK, Brooks RP, Ehrensberger MT, Effects of simulated inflammation on the corrosion of 316L stainless steel, Mat Sci Eng C-Mater 71 (2017) 200–205.

[85]. Dorozhkin SV, Calcium orthophosphate coatings on magnesium and its biodegradable alloys, Acta Biomater. 10(7) (2014) 2919–34. [PubMed: 24607420]

[86]. Hornberger H, Virtanen S, Boccaccini AR, Biomedical coatings on magnesium alloys - a review, Acta Biomater. 8(7) (2012) 2442–55. [PubMed: 22510401]

[87]. Liu B, Zhang X, Xiao GY, Lu YP, Phosphate chemical conversion coatings on metallic substrates for biomedical application: a review, Mater Sci Eng C Mater Biol Appl 47 (2015) 97–104. [PubMed: 25492177]

[88]. Su Y, Cockerill I, Zheng Y, Tang L, Qin YX, Zhu D, Biofunctionalization of metallic implants by calcium phosphate coatings, Bioact Mater 4 (2019) 196–206. [PubMed: 31193406]

[89]. Chu PW, Marquis EA, Linking the microstructure of a heat-treated WE43 Mg alloy with its corrosion behavior, Corros. Sci 101 (2015) 94–104.

[90]. Ascencio M, Pekguleryuz M, Omanovic S, An investigation of the corrosion mechanisms of WE43 Mg alloy in a modified simulated body fluid solution: The influence of immersion time, Corros. Sci 87 (2014) 489–503.

[91]. Liu D, Yang D, Li X, Hu S, Mechanical properties, corrosion resistance and biocompatibilities of degradable Mg-RE alloys: A review, Journal of Materials Research and Technology (2018).

[92]. Marx SO, Totary-Jain H, Marks AR, Vascular smooth muscle cell proliferation in restenosis, Circ Cardiovasc Interv 4(1) (2011) 104–11. [PubMed: 21325199]

[93]. Wang GX, Ge SP, Shen Y, Wang HG, Dong QL, Zhang Q, Gao JC, Wang Y, Study on the biodegradability and biocompatibility of WE magnesium alloys, Mat Sci Eng C-Mater 32(8) (2012) 2190–2198.

[94]. Zhen Z, Liu X, Huang T, Xi T, Zheng Y, Hemolysis and cytotoxicity mechanisms of biodegradable magnesium and its alloys, Mater Sci Eng C Mater Biol Appl 46 (2015) 202–6. [PubMed: 25491978]

[95]. Levy G. Katarivas, Kafri A, Ventura Y, Leon A, Vago R, Goldman J, Aghion E, Surface stabilization treatment enhances initial cell viability and adhesion for biodegradable zinc alloys, Mater. Lett 248 (2019) 130–133.

[96]. Jablonska E, Vojtech D, Fousova M, Kubasek J, Lipov J, Fojt J, Ruml T, Influence of surface pre-treatment on the cytocompatibility of a novel biodegradable ZnMg alloy, Mater Sci Eng C Mater Biol Appl 68 (2016) 198–204. [PubMed: 27524013]

[97]. Lorenz C, Brunner JG, Kollmannsberger P, Jaafar L, Fabry B, Virtanen S, Effect of surface pre-treatments on biocompatibility of magnesium, Acta Biomater. 5(7) (2009) 2783–9. [PubMed: 19427423]

[98]. Su Y, Yang H, Gao J, Qin YX, Zheng Y, Zhu D, Interfacial Zinc Phosphate is the Key to Controlling Biocompatibility of Metallic Zinc Implants, Adv Sci (Weinh) 6(14) (2019) 1900112. [PubMed: 31380203]

[99]. Liang C, Hu Y, Wang H, Xia D, Li Q, Zhang J, Yang J, Li B, Li H, Han D, Dong M, Biomimetic cardiovascular stents for in vivo re-endothelialization, Biomaterials 103 (2016) 170–182. [PubMed: 27380443]

[100]. Biela SA, Su Y, Spatz JP, Kemkemer R, Different sensitivity of human endothelial cells, smooth muscle cells and fibroblasts to topography in the nano-micro range, Acta Biomater. 5(7) (2009) 2460–6. [PubMed: 19410529]

[101]. Xu CY, Inai R, Kotaki M, Ramakrishna S, Aligned biodegradable nanotibrous structure: a potential scaffold for blood vessel engineering, Biomaterials 25(5) (2004) 877–886. [PubMed: 14609676]

[102]. Shahryari A, Azari F, Vali H, Omanovic S, The response of fibrinogen, platelets, endothelial and smooth muscle cells to an electrochemically modified SS316LS surface: towards the enhanced biocompatibility of coronary stents, Acta Biomater. 6(2) (2010) 695–701. [PubMed: 19607940]

[103]. Yang Z, Tu Q, Zhu Y, Luo R, Li X, Xie Y, Maitz MF, Wang J, Huang N, Mussel-inspired coating of polydopamine directs endothelial and smooth muscle cell fate for re-endothelialization of vascular devices, Adv Healthc Mater 1(5) (2012) 548–59. [PubMed: 23184789]

[104]. Liu XW, Sun JK, Yang YH, Pu ZJ, Zheng YF, In vitro investigation of ultra-pure Zn and its mini-tube as potential bioabsorbable stent material, Mater Lett 161 (2015) 53–56.

[105]. Ma J, Zhao N, Zhu D, Bioabsorbable zinc ion induced biphasic cellular responses in vascular smooth muscle cells, Scientific reports 6 (2016) 26661. [PubMed: 27248371]

[106]. Zhao N, Zhu D, Endothelial responses of magnesium and other alloying elements in magnesium-based stent materials, Metallomics : integrated biometal science 7(1) (2015) 118–28. [PubMed: 25363018]

[107]. Shearier ER, Bowen PK, He WL, Drench A, Drelich J, Goldman J, Zhao F, In Vitro Cytotoxicity, Adhesion, and Proliferation of Human Vascular Cells Exposed to Zinc, Acs Biomater Sci Eng 2(4) (2016) 634–642. [PubMed: 27840847]

[108]. Heublein B, Rohde R, Kaese V, Niemeyer M, Hartung W, Haverich A, Biocorrosion of magnesium alloys: a new principle in cardiovascular implant technology?, Heart 89(6) (2003) 651–656. [PubMed: 12748224]

[109]. Hanzi AC, Gerber I, Schinhammer M, Loffler JF, Uggowitzer PJ, On the in vitro and in vivo degradation performance and biological response of new biodegradable Mg-Y-Zn alloys, Acta Biomaterialia 6(5) (2010) 1824–1833. [PubMed: 19815099]

[110]. Bowen PK, Seitz JM, Guillory RJ, Braykovich JP, Zhao S, Goldman J, Drelich JW, Evaluation of wrought Zn-Al alloys (1, 3, and 5 wt % Al) through mechanical and in vivo testing for stent applications, J Biomed Mater Res B 106(1) (2018) 245–258.

[111]. Pierson D, Edick J, Tauscher A, Pokorney E, Bowen P, Gelbaugh J, Stinson J, Getty H, Lee CH, Drelich J, Goldman J, A simplified in vivo approach for evaluating the bioabsorbable behavior of candidate stent materials, J Biomed Mater Res B 100b(1) (2012) 58–67.

[112]. Bowen PK, Guillory RJ, Shearier ER, Seitz JM, Drelich J, Bocks M, Zhao F, Goldman J, Metallic zinc exhibits optimal biocompatibility for bioabsorbable endovascular stents, Mat Sci Eng C-Mater 56 (2015) 467–472.

[113]. Zhao S, Seitz JM, Eifler R, Maier HJ, Guillory RJ, Earley EJ, Drelich A, Goldman J, Drelich JW, Zn-Li alloy after extrusion and drawing: Structural, mechanical characterization, and biodegradation in abdominal aorta of rat, Mat Sci Eng C-Mater 76 (2017) 301–312.

[114]. Bowen PK, Drelich J, Goldman J, Zinc Exhibits Ideal Physiological Corrosion Behavior for Bioabsorbable Stents, Advanced Materials 25(18) (2013) 2577–2582. [PubMed: 23495090]

[115]. Bowen PK, Drelich J, Buxbaum RE, Rajachar RM, Goldman J, New approaches in evaluating metallic candidates for bioabsorbable stents, Emerg Mater Res 1(5) (2012) 237–255.

[116]. Holmes DR, State of the art in coronary intervention, American Journal of Cardiology 91(3) (2003) 50a–53a.

[117]. Fischman DL, Leon MB, Baim DS, Schatz RA, Savage MP, Penn I, Detre K, Veltri L, Ricci D, Nobuyoshi M, Cleman M, Heuser R, Almond D, Teirstein PS, Fish RD, Colombo A, Brinker J, Moses J, Shaknovich A, Hirshfeld J, Bailey S, Ellis S, Rake R, Goldberg S, A Randomized Comparison of Coronary-Stent Placement and Balloon Angioplasty in the Treatment of

Coronary-Artery Disease, New England Journal of Medicine 331(8) (1994) 496–501. [PubMed: 8041414]

[118]. Serruys PW, de Jaegere P, Kiemeneij F, Macaya C, Rutsch W, Heyndrickx G, Emanuelsson H, Marco J, Legrand V, Materne P, et al., A comparison of balloon-expandable-stent implantation with balloon angioplasty in patients with coronary artery disease. Benestent Study Group, N Engl J Med 331(8) (1994) 489–95. [PubMed: 8041413]

[119]. Schmidmaier G, Lucke M, Wildemann B, Haas NP, Raschke M, Prophylaxis and treatment of implant-related infections by antibiotic-coated implants: a review, Injury 37 Suppl 2(2) (2006) S105–12. [PubMed: 16651063]

[120]. Wang YW, Cao A, Jiang Y, Zhang X, Liu JH, Liu Y, Wang H, Superior antibacterial activity of zinc oxide/graphene oxide composites originating from high zinc concentration localized around bacteria, ACS Appl Mater Interfaces 6(4) (2014) 2791–8. [PubMed: 24495147]

[121]. Zhu P, Weng ZY, Li X, Liu XM, Wu SL, Yeung KWK, Wang XB, Cui ZD, Yang XJ, Chu PK, Biomedical Applications of Functionalized ZnO Nanomaterials: from Biosensors to Bioimaging, Advanced Materials Interfaces 3(1) (2016).

[122]. Zou YH, Wang J, Cui LY, Zeng RC, Wang QZ, Han QX, Qiu J, Chen XB, Chen DC, Guan SK, Zheng YF, Corrosion resistance and antibacterial activity of zinc-loaded montmorillonite coatings on biodegradable magnesium alloy AZ31, Acta Biomater. (2019).

[123]. Xiang Y, Mao C, Liu X, Cui Z, Jing D, Yang X, Liang Y, Li Z, Zhu S, Zheng Y, Yeung KWK, Zheng D, Wang X, Wu S, Rapid and Superior Bacteria Killing of Carbon Quantum Dots/ZnO Decorated Injectable Folic Acid-Conjugated PDA Hydrogel through Dual-Light Triggered ROS and Membrane Permeability, Small 15(22) (2019) e1900322. [PubMed: 31021489]

[124]. Feng YH, Liu L, Zhang J, Aslan H, Dong MD, Photoactive antimicrobial nanomaterials, Journal of Materials Chemistry B 5(44) (2017) 8631–8652.

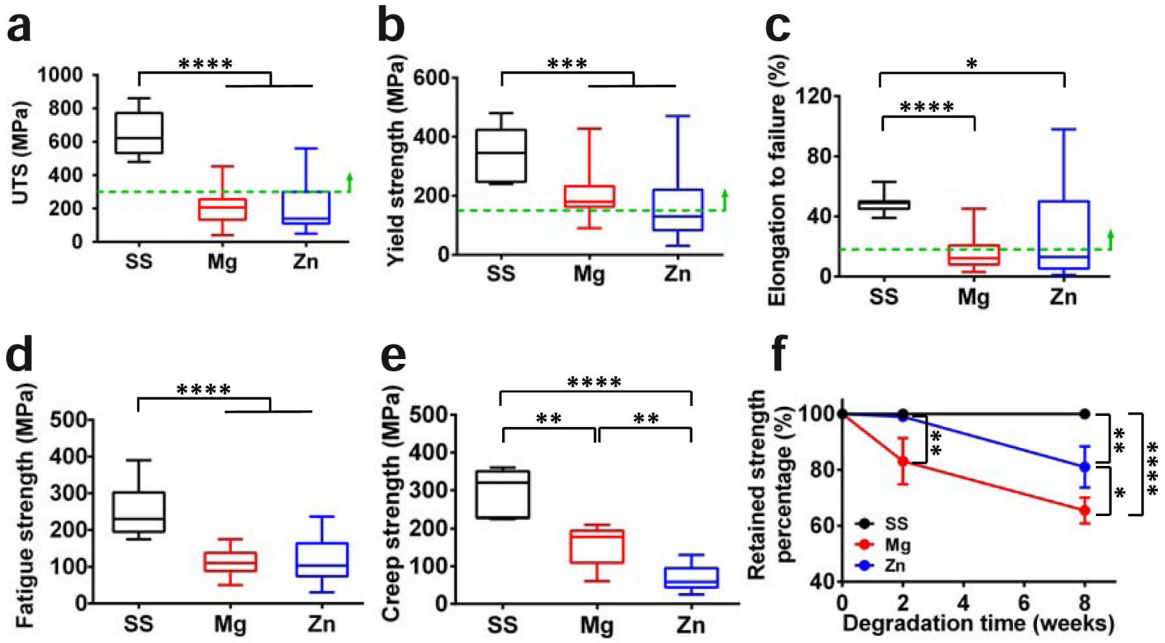

Fig. 1.

Mechanical properties of SS, Mg, and Zn based metallic materials summarized from prior published work [19, 33, 50–71]. (a) Ultimate tensile strength (UTS), (b) yield strength, (c) elongation to failure, (d) fatigue strength, (e) creep strength, and (f) the percentage of retained strength with degradation time. The approximate mechanical benchmarks required for stent materials are marked by the green dashed lines. *$p < 0.05$, ** $p < 0.01$, *** $p < 0.001$, **** $p < 0.0001$, compared between groups.

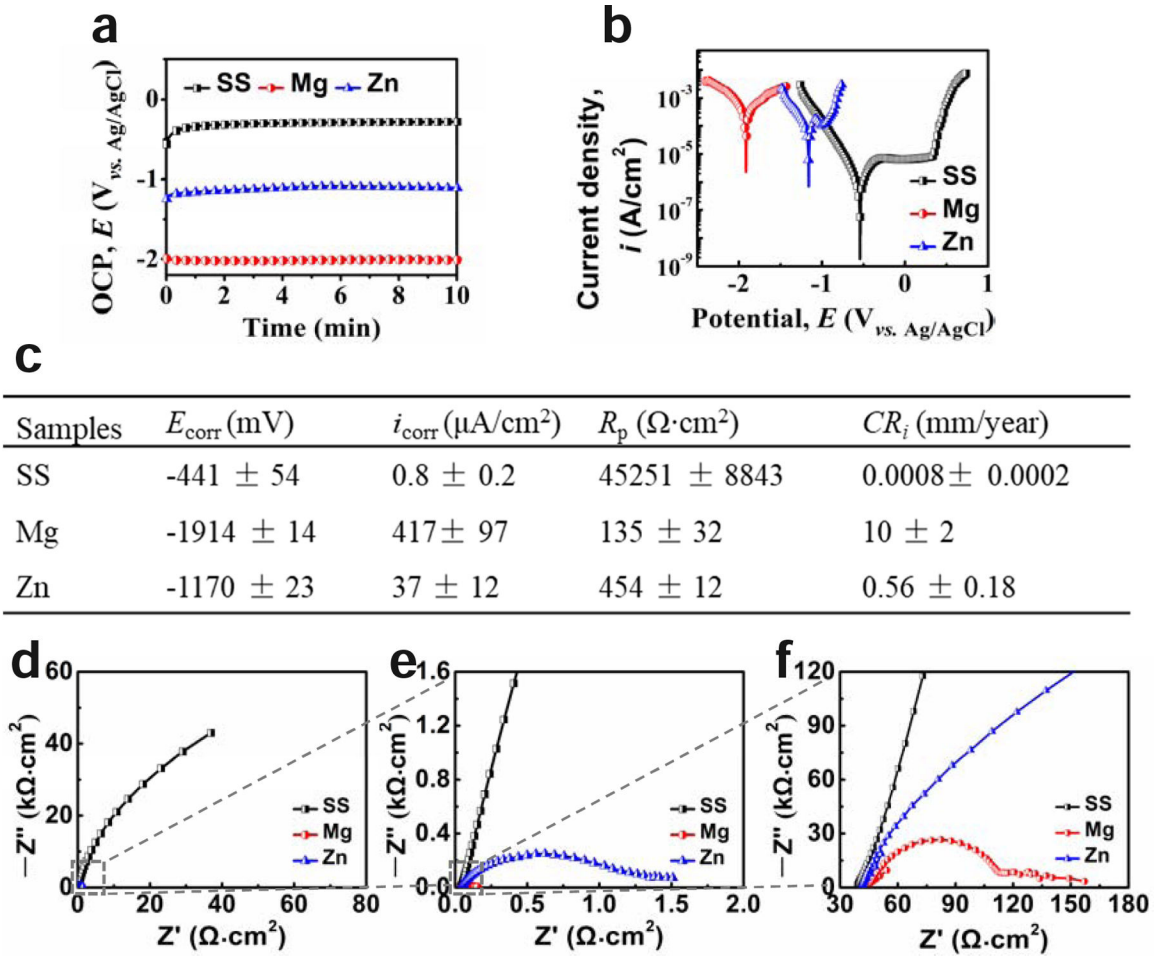

Samples	E_{corr} (mV)	i_{corr} (μA/cm²)	R_p (Ω·cm²)	CR_i (mm/year)
SS	-441 ± 54	0.8 ± 0.2	45251 ± 8843	0.0008 ± 0.0002
Mg	-1914 ± 14	417 ± 97	135 ± 32	10 ± 2
Zn	-1170 ± 23	37 ± 12	454 ± 12	0.56 ± 0.18

Fig. 2.

Electrochemical corrosion behaviors of SS, Mg, and Zn samples in Hank's solution. (a) open circuit potential (OCP), (b) potentiodynamic polarization, (c) corrosion parameters obtained from (b), (d-f) Electrochemical impedance spectroscopy (EIS), (e) and (f) are the enlarged squares in (d) and (e), respectively.

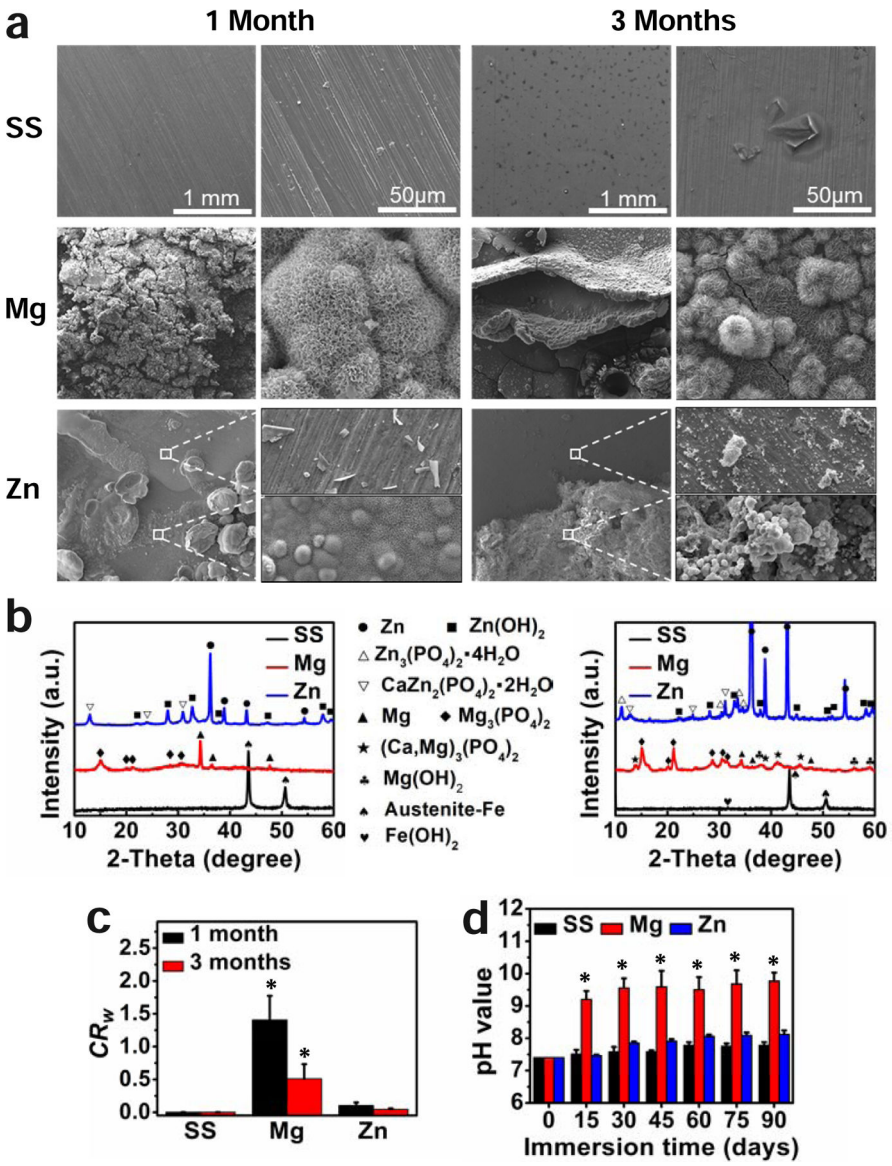

Fig. 3.

Immersion degradation analyses of SS, Mg, and Zn samples in Hank's solution for 1 and 3 months. (a) Degraded surface morphology, (b) XRD patterns, (c) corrosion rate, (d) pH values with immersion time. *$p < 0.05$, compared with the other two material groups.

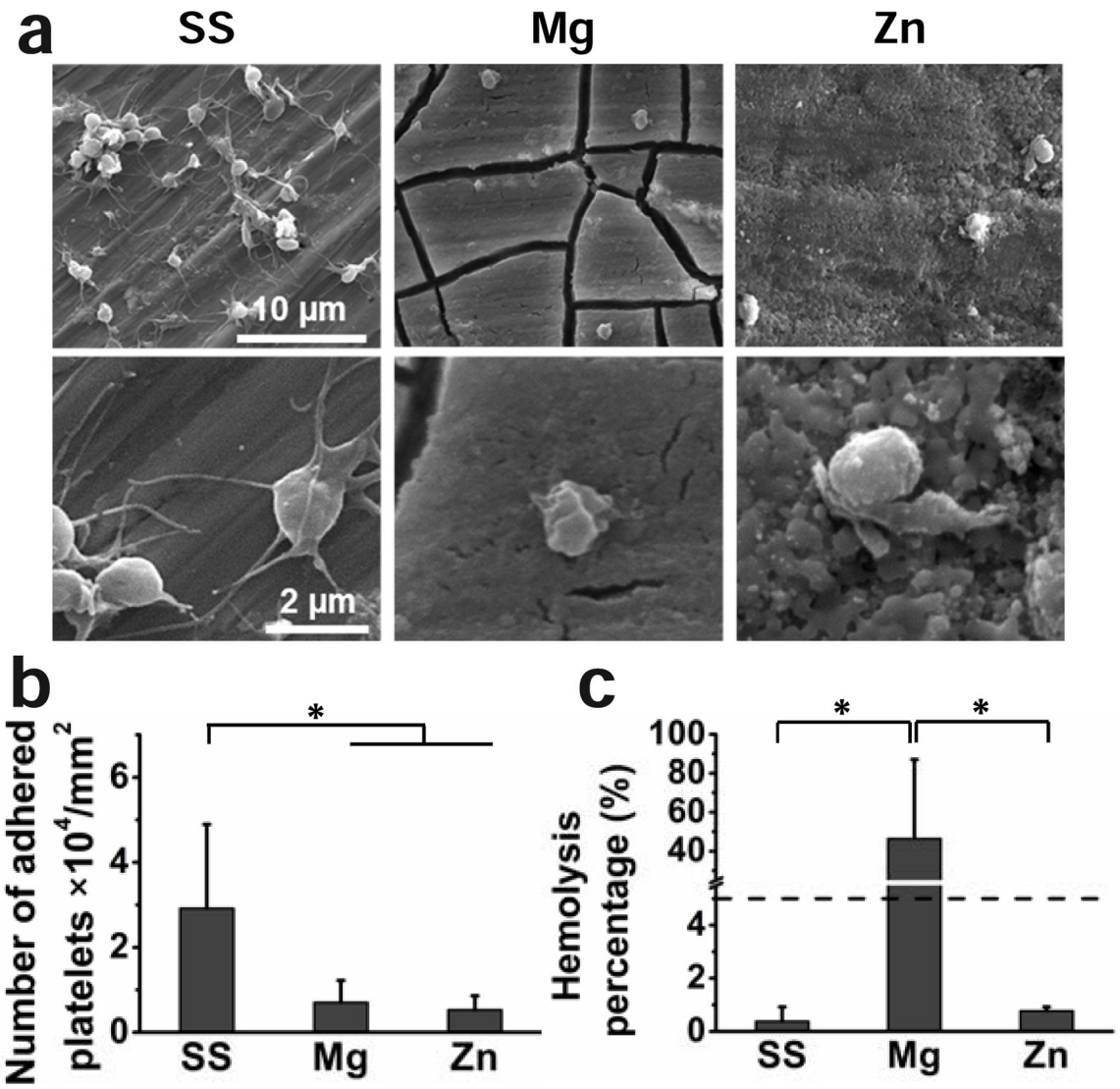

Fig. 4.

Hemocompatibility of SS, Mg, and Zn samples. (a) Platelets adhesion morphology on SS, Mg and Zn materials, (b) the corresponding number of adhered platelets, (c) hemolysis percentage. *$p < 0.05$, compared between groups.

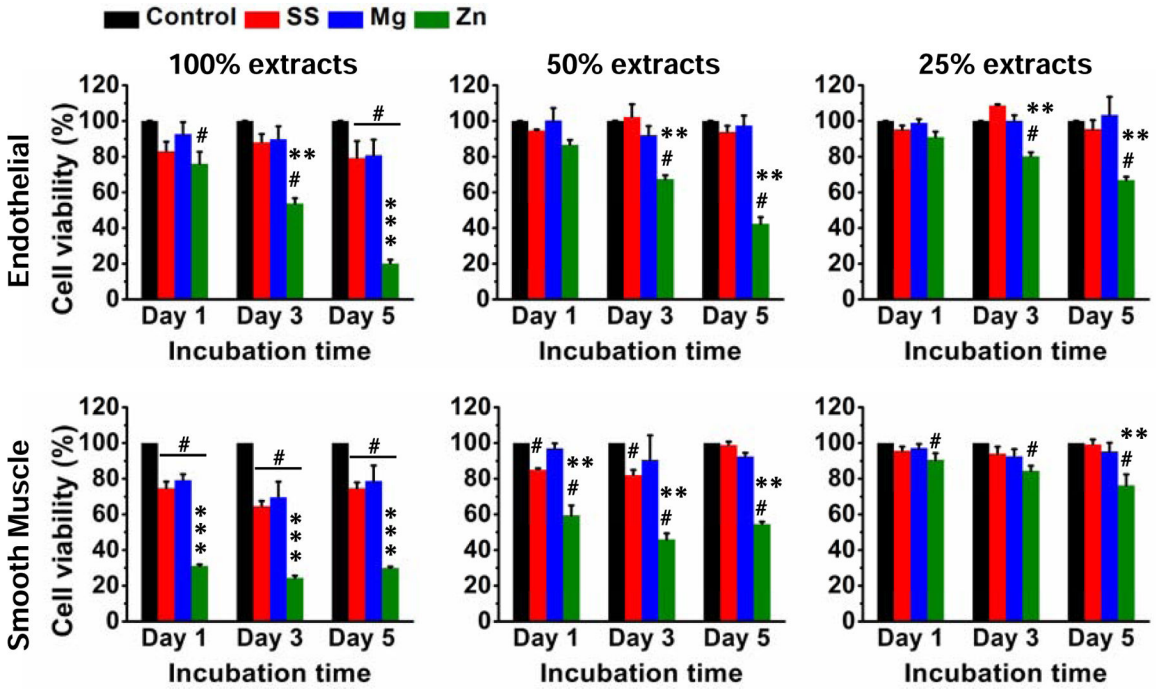

Fig. 5.

Cell viability of endothelial and smooth muscle cells cultured with different concentrations of extracts from SS, Mg, and Zn samples. #$p < 0.01$, compared with control group; **$p < 0.01$, *** $p < 0.001$, compared with the other two material groups.

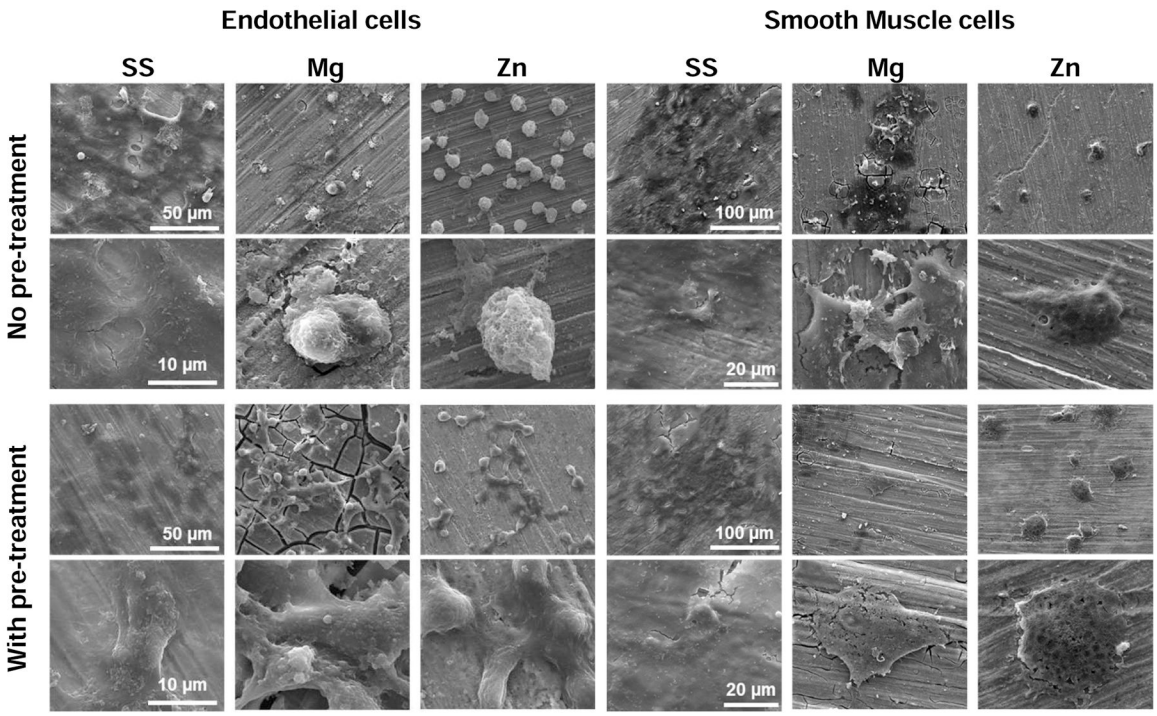

Fig. 6.

Cell adhesion morphology on SS, Mg, and Zn samples with or without pretreatment in the cell culture media for 3 days.

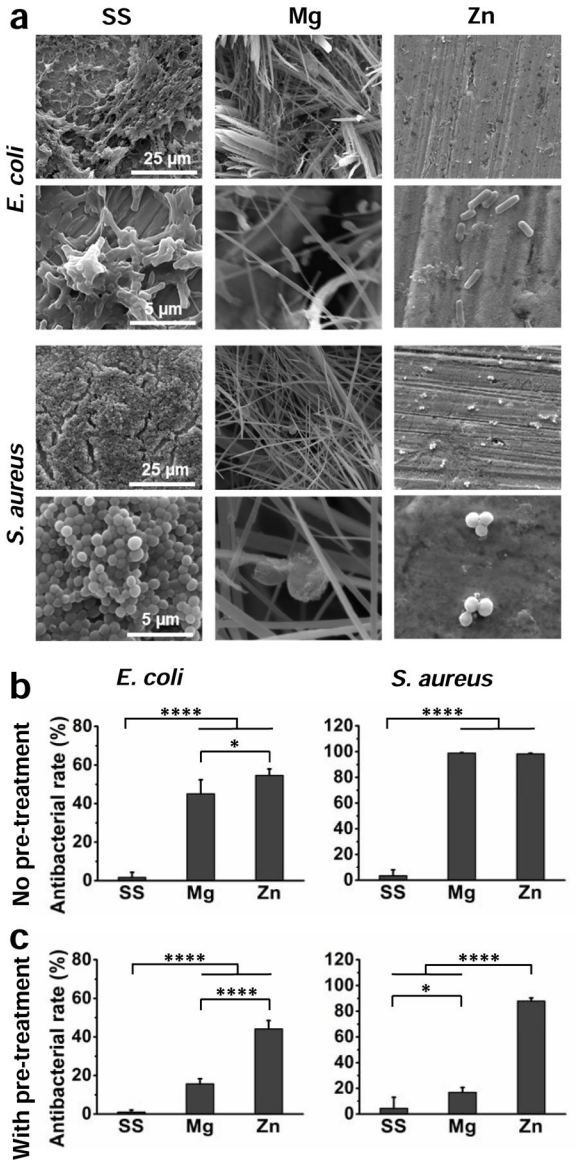

Fig. 7.

Antibacterial performance of SS, Mg, and Zn samples cultured with *E. coli* and *S. aureus* for 24 h. (a) SEM images of bacterial adhesion on sample surfaces. (b) Antibacterial rates in the culture medium without surface pretreatment. (c) Antibacterial rates in the culture medium with surface pretreatment. *$p < 0.05$, **** $p < 0.0001$, compared between groups.

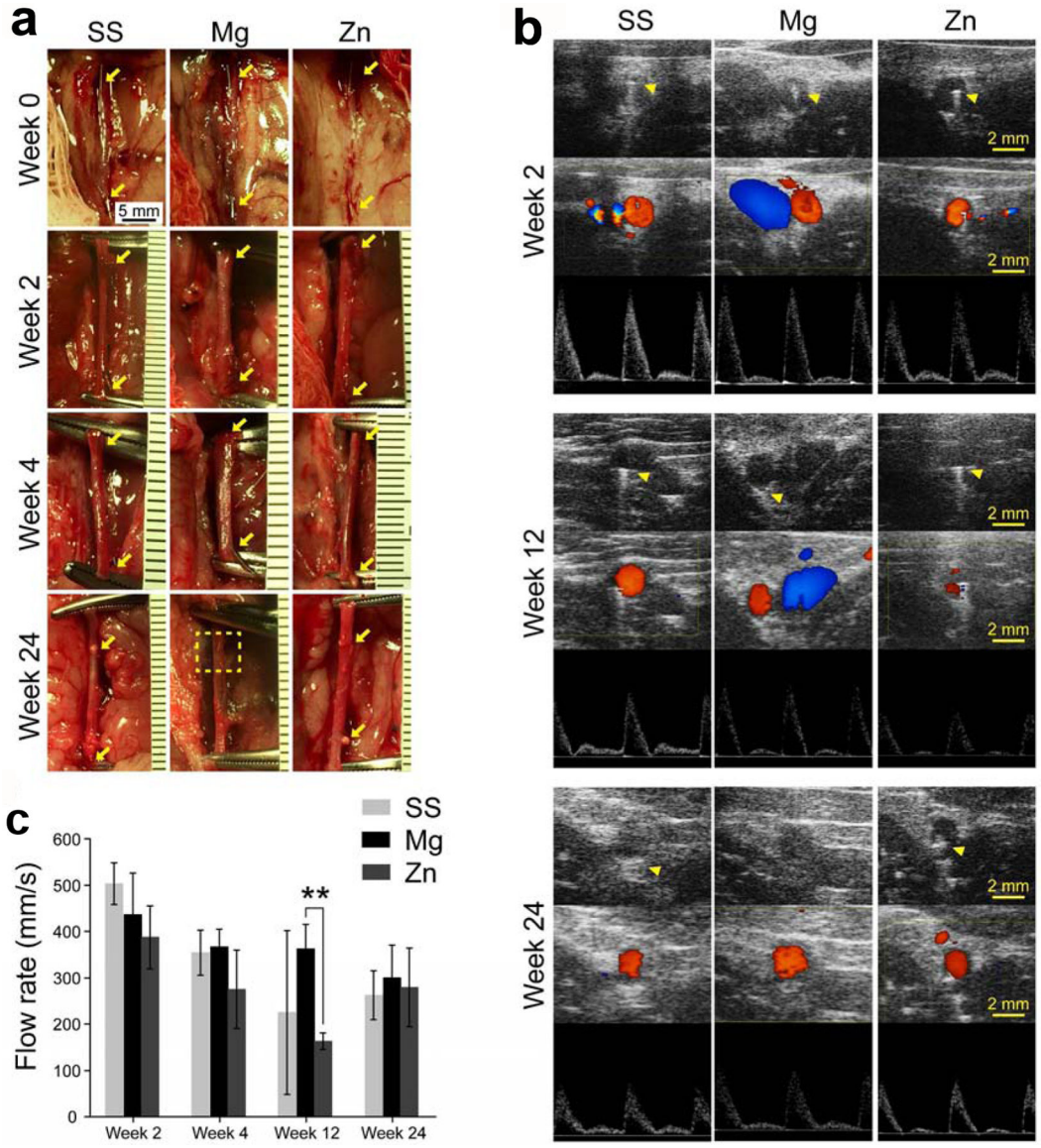

Fig. 8.

(a) Macroscopic view of metallic wires in rat abdominal aortas right after implantation and before explantation. Arrow heads indicate the ends of the implanted wires. Dash square indicates the residue of Mg residuals after complete absorption. (b) Ultrasound images of rat abdominal aorta. Upper: B mode; middle: Doppler mode; Lower: PW mode. Arrow heads indicate ultrasound shadow of the implanted metallic wires. (c) Flow rate of blood in rat abdominal aortas where samples were implanted. ** $p < 0.01$, compared between two groups.

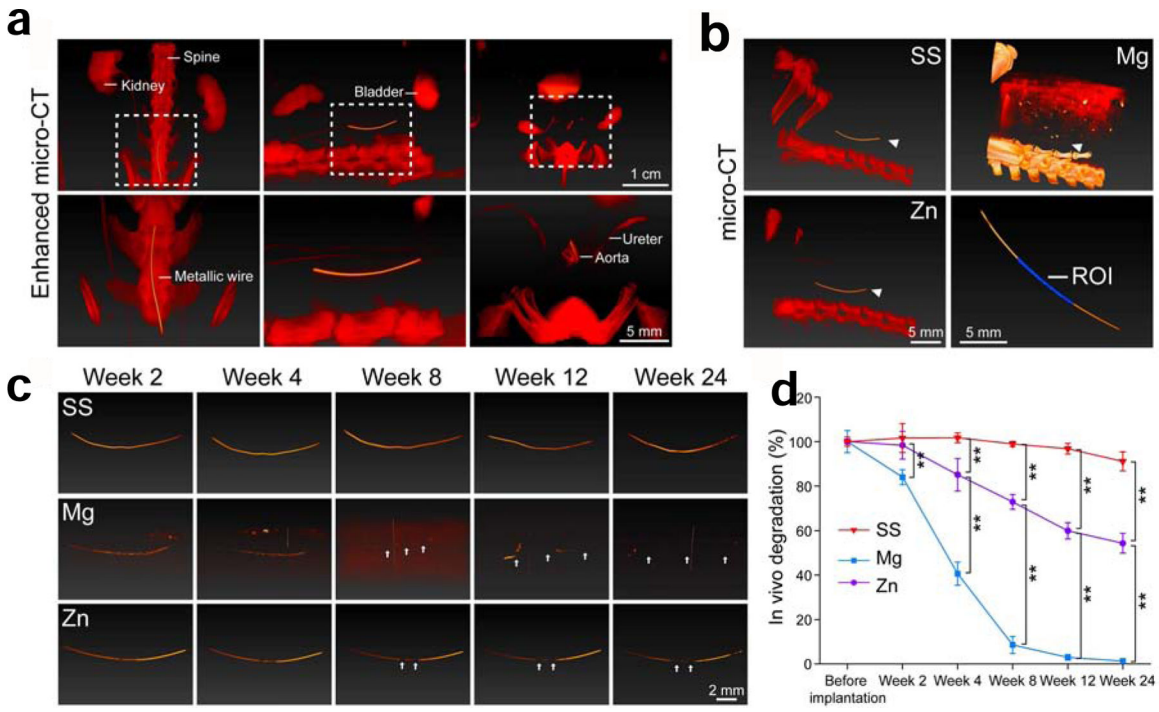

Fig. 9.

(a) Representative images of enhanced μCT from different views. Left: front view; Middle: side view; Right: cross-section view. Contrast reagents were used for the enhanced μCT and are indicated in red color. (b) Representative images of μCT in different groups. Arrow heads indicate the implanted metallic wires. ROI: region of interest. (c) Representative images of the implanted metallic wires. Arrow heads indicate the notch of degradation on the implanted metallic wires. (d) The in vivo degradation of metallic wires in rat abdominal aortas. $^{**}p < 0.01$, compared between two groups.

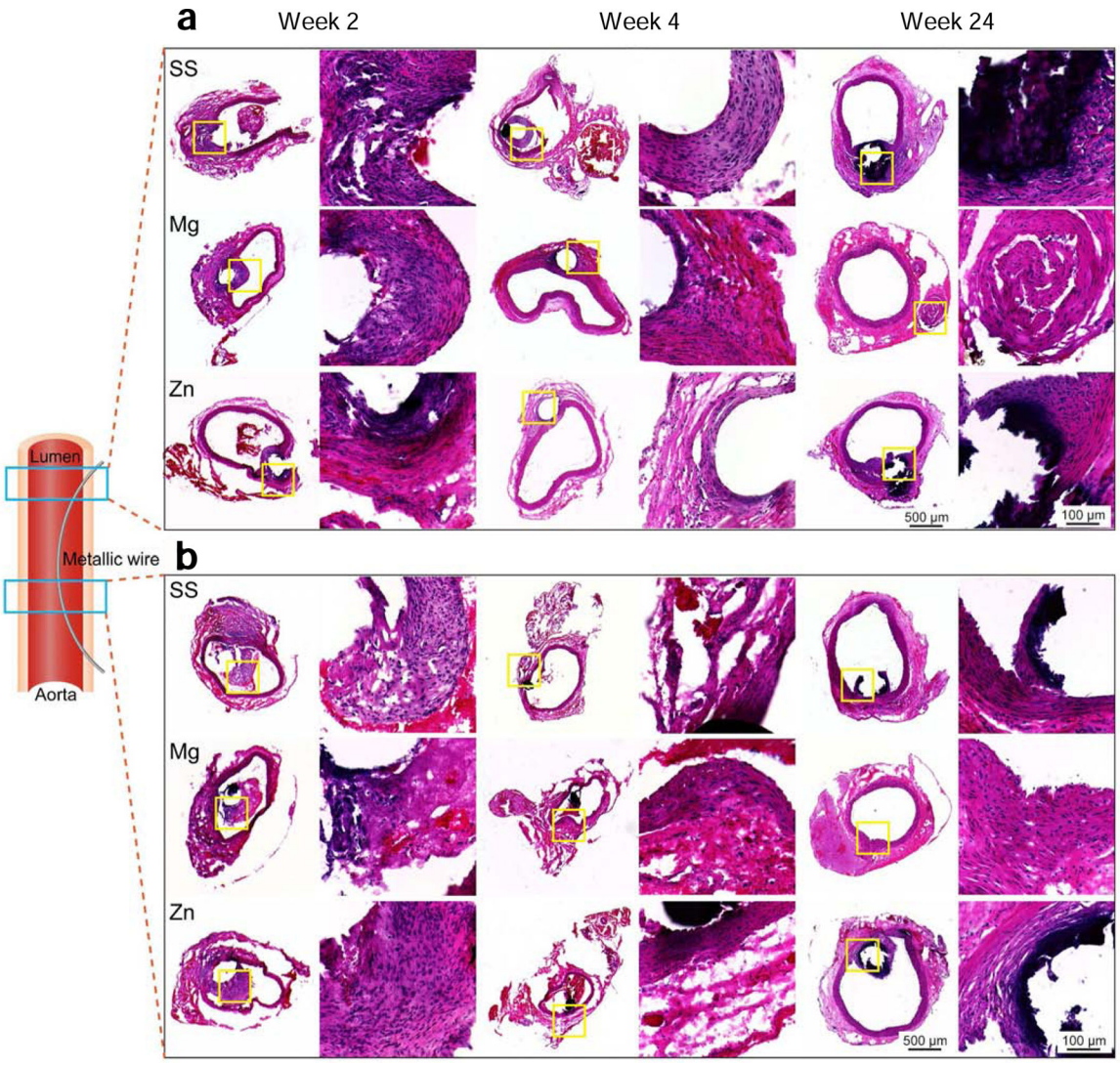

Fig. 10.

H&E staining of aortas and implants. (a) Vascular walls with metallic wire insertion. (b) Aortas at the site where metallic wires were in the lumen.

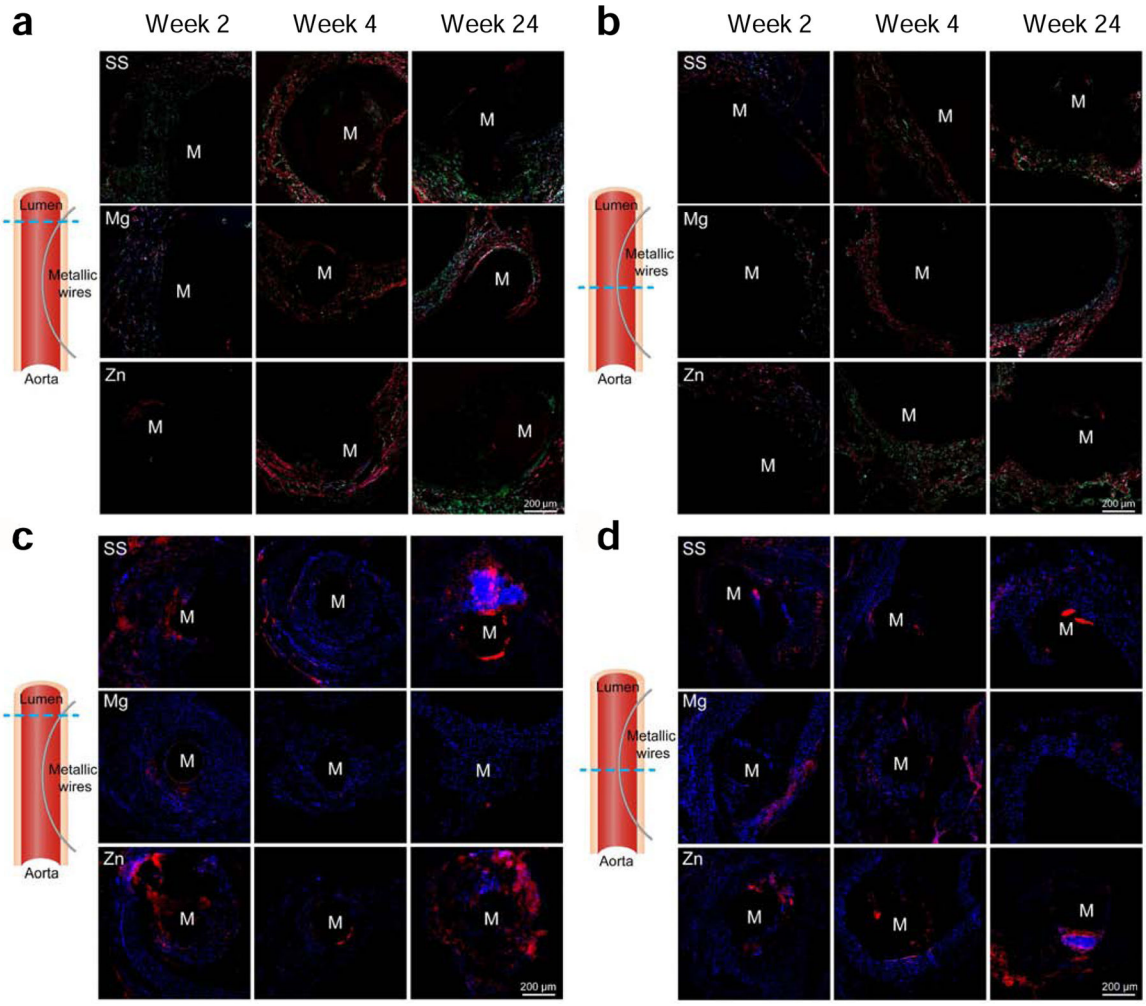

Fig. 11.

(a-b) Picro sirius red staining and (c-d) CD11b immunofluorescent staining of aortas and implants. (a, c) Vascular walls with metallic wire insertion. (b, d) Aortas at the site where metallic wires were in the lumen. (a-b) Images are taken under polarized light. Yellow-orange birefringence indicates thick collagen fibers and green birefringence indicate thin type III collagen fibers. (c-d) Blue colors indicate nucleus and red colors indicate positive staining.

Table 1.

Summary of *in vitro* and *in vivo* properties of SS, Mg and Zn as cardiovascular stent materials.

Property		SS	Mg	Zn
Mechanical	Static strength and ductility	High	Low	Medium
	Fatigue strength	High	Low	Low
	Creep strength	High	Medium	Low
	Mechanical stability with degradation	High	Low	Medium
Degradation	Degradation *in vitro*	Quite slow	Fast	Medium
	Degradation *in vivo* (6 month)	10%	100%	40%
Biocompatibility	Platelets adhesion	Activated	Inhibited	Inhibited
	Hemolysis	Low	High	Low
	Hemocompatibility *in vivo* (Ultrasound)	Good	Good	Good
	Endothelial cell adhesion	Good	Good	Good
	Smooth muscle cell adhesion	Activated	Inhibited	Inhibited
	Inflammation responses *in vivo*	Strong	Mild	Strong
Antibacterial	*E. coli*	Bad	Good (*in vitro*)	Good
	S. aureus	Bad	Good (*in vitro*)	Good